Structural building principles of complex face-centered cubic intermetallics

Julia Dshemuchadse, Daniel Y. Jung and Walter Steurer*

Laboratory of Crystallography, Department of Materials, ETH Zurich, Wolfgang-Pauli-Strasse 10, 8093 Zurich, Switzerland

Correspondence e-mail: steurer@mat.ethz.ch

Fundamental structural building principles are discussed for all 56 known intermetallic phases with approximately 400 or more atoms per unit cell and space-group symmetry $F\bar{4}3m$, $Fd\bar{3}m$, $Fd\bar{3}$, $Fm\bar{3}m$ or $Fm\bar{3}c$. Despite fundamental differences in chemical composition, bonding and electronic band structure, their complex crystal structures show striking similarities indicating common building principles. We demonstrate that the structure-determining elements are flat and puckered atomic {110} layers stacked with periodicities $2p$. The atoms on this set of layers, which intersect each other, form pentagon face-sharing endohedral fullerene-like clusters arranged in a face-centered cubic packing (f.c.c.). Due to their topological layer structure, all these crystal structures can be described as $(p \times p \times p) = p^3$-fold superstructures of a common basic structure of the double-diamond type. The parameter p, with $p = 3, 4, 7$ or 11, is determined by the number of layers per repeat unit and the type of cluster packing, which in turn are controlled by chemical composition.

1. Introduction

Why and how do complex intermetallic phases form with up to thousands of atoms per unit cell or even in a quasiperiodic way without a unit cell? How do all these atoms find their sites during crystal growth? How do their structures depend on chemical composition and do they have anything in common? All these questions are in the focus of our long-term study of the crystallography of complex intermetallics, periodic as well as quasiperiodic ones. In this first comprehensive classification of intermetallics with giant unit cells, we discuss all known f.c.c. structures in the range from approximately 400 up to more than 23 000 atoms per unit cell.

Structural complexity can result from:

(i) atomic size ratios geometrically hindering optimum atomic interactions and preventing the formation of atomic environment types (AETs), which can be packed efficiently;

(ii) energetically favorable electronic band structures (*e.g.* pseudogaps at the Fermi energy, E_F) based on odd stoichiometries or large unit-cell dimensions;

(iii) other parameters that are close to optimum but not optimum (pseudosymmetry) for a simple structural arrangement or packing such as a misfit between structural subunits as in composite (host/guest) or modulated structures.

In some cases complex structures can be described as modulations or superstructures of rather simple basic structures. We distinguish two classes of modulations: a *simple modulation* is a correlated displacement or substitution of atoms leading to a comparatively small deviation of the actual structure from the underlying basic structure, resulting in a (in)commensurately modulated structure. A *complex modula-*

tion on the other hand results from a correlated displacement or substitution of atoms leading to the local formation of clusters yielding a *cluster-modulated structure*; as we will show, this is the case for all structures discussed in the following.

There is no unique way to classify, describe and visualize the crystal structure of a complex intermetallic compound. One should keep in mind that the visualization of a crystal structure in terms of clusters (in the meaning of structural building blocks) or structure modules can be quite arbitrary. There are some conventions and rules, such as the maximum-gap rule (Brunner & Schwarze, 1971) for the definition of AETs, which can be seen, in some cases, as the first shell of a multi-shell cluster. However, there are not usually such simple rules for higher-order cluster shells. Furthermore, even if one finds a topologically elucidating cluster-based description, this does not mean that it is supported from a crystal-chemical point of view, *i.e.* that the chemical bonds between atoms within a cluster differ from those outside a cluster. For a more detailed discussion of this problem see Steurer (2006) and Henley *et al.* (2006).

In the following we will pragmatically utilize this kind of cluster description that proves to be most useful. This is the case when it allows for a simpler representation of a structure which is simpler than any other geometrical description; it is particularly justified if the clusters used are constituents of more than just a single structure type. A useful cluster-based description relates complex structures to simpler ones, thereby reducing the degree of complexity and unveiling the underlying packing principles. In this case of f.c.c. structures, the fundamental endohedral pentagon face-sharing fullerene-like clusters form cubic close packing with the octahedral voids filled with a second type of cluster. The choice of this kind of cluster is particularly justified because it allows the family of giant unit-cell structures $cF444$-$Al_{63.6}Ta_{36.4}$, $cF(5928 - x)$-$Al_{56.6}Cu_{3.9}Ta_{39.5}$ and $cF(23256 - x)$-$Al_{55.4}Cu_{5.4}Ta_{39.1}$ (Weber *et al.*, 2009; Conrad *et al.*, 2009) to be described in a unique way.
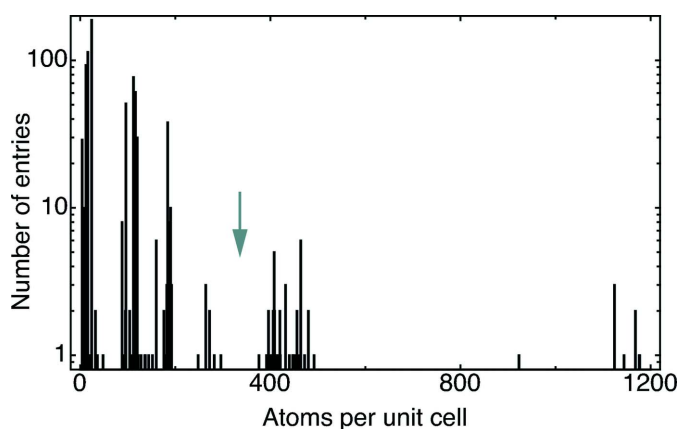

Figure 1
Occurrence of f.c.c. intermetallic structures as a function of the number of atoms per unit cell, created from the 1518 PCD entries with completely determined structures. The batch size of the histogram is four atoms. All structures beyond the gap marked by the arrow are discussed in the present paper.

We want to emphasize that our goal is the crystallographic description of complex structures, to identify their structural building units and connectivities. A detailed analysis of chemical bonding and the identification of chemically relevant subunits such as polyanionic frameworks is beyond the scope of this study.

The paper is organized in the following way: in §2 we describe the data basis of the present study and introduce the general packing principles and peculiarities we derived for f.c.c. structures with giant unit cells; in §§3, 4 and 5 we apply our concept of cluster description, layer decomposition and average structure derivation to the 56 intermetallics grouped according to their symmetries $F\bar{4}3m$ (39), $Fd\bar{3}m$ (9), $Fd\bar{3}$ (1), $Fm\bar{3}m$ (4) or $Fm\bar{3}c$ (3); in §6 we discuss the results of *ab initio* calculations of representatives of the two most frequent structure types and show that chemical bonding and electronic band structure differ significantly between all these geometrically closely related structures.

2. Some peculiarities of complex f.c.c. intermetallics

Our study is based on structures taken from Pearson's Crystal Data database (PCD; Villars & Cenzual, 2009/10). Full structural information is only available for 10 655 of the 41 788 intermetallics[1] included in this database. However, these numbers refer to database entries and not necessarily to structures of different compounds; for some compounds, more than one entry may exist based on different structure determinations. We restrict our study to the fully determined structures and start with the analysis of 1891 entries with cubic symmetry and focus first on the 842 with f.c.c. lattice symmetry: $Fm\bar{3}$ (4 entries), $Fd\bar{3}$ (1 entry), $F\bar{4}3m$ (305 entries), $Fm\bar{3}m$ (249 entries), $Fm\bar{3}c$ (76 entries) and $Fd\bar{3}m$ (207 entries).[2]

The histogram in Fig. 1 lists the number of database entries of f.c.c. structures as a function of the number of atoms per unit cell. Obviously, the majority of f.c.c. structures has unit cells with less than 200 atoms. Another significant clustering of structures is found at around 400 atoms per unit cell, while even larger structures are sparse. These are the structures we will focus on in the following, taking into account both their comparably high frequency and complexity. In this survey, we also consider the two recently discovered structures $cF(5928 - x)$-$Al_{56.6}Cu_{3.9}Ta_{39.5}$ and $cF(23256 - x)$-$Al_{55.4}Cu_{5.4}Ta_{39.1}$ (Weber *et al.*, 2009; Conrad *et al.*, 2009), with space-group symmetry $F\bar{4}3m$, which are not included in the databases yet, as well as structures taken directly from the literature and another database, the ICSD (Belsky *et al.*, 2002). Most of the 56 structures selected (Table 1) belong to just two space groups, $F\bar{4}3m$ and $Fd\bar{3}m$, with 39 and 9 entries. $Fd\bar{3}$, $Fm\bar{3}m$ and $Fm\bar{3}c$ are represented altogether by eight entries only. These 56 complex intermetallics differ strongly in their

Table 1

All 56 f.c.c. complex intermetallics discussed in this work.

Given are the space group and the type of superstructure, as well as the normalized composition, the unit-cell parameter a, Pearson symbol and references.

Composition	a (°A)	Pearson	Reference
$F\bar{4}3m$, $(3 \times 3 \times 3)$-fold superstructures (36), 4 subtypes, $cF(456 - x)$			
Subtype I	(14 structures)	$cF(432 - x)$	
$Li_{64.3}In_{26.5}Ag_{9.2}$	20.089	$cF432$	(a)
$Li_{81.0}Pb_{19.0}$	19.842	$cF420$	(b)
$Li_{81.0}Sn_{19.0}$	19.6907	$cF420$	(b)
$Li_{81.0}Ge_{19.0}$	18.756	$cF(420 - 1)$	(b)
$Zn_{80.9}Pd_{14.5}Al_{4.6}$	18.1600	$cF416$	(c)
$Zn_{82.7}Pt_{17.3}$	18.14	$cF(416 - 16)$	(d)
$Zn_{81.6}Pt_{18.4}$	18.128	$cF416$	(d)
$Zn_{78.7}Pd_{16.0}Al_{5.3}$	18.113	$cF(416 - 9)$	(c)
$Zn_{77.0}Pt_{23.0}$	18.1128	$cF(392 - 16)$	(e)
$Zn_{80.0}Pt_{20.0}$	18.091	$cF(416 - 8)$	(d)
$Zn_{78.5}Pd_{14.0}Al_{7.5}$	18.0700	$cF400$	(c)
$Cu_{73.9}Sn_{23.2}Ni_{2.9}$	18.011	$cF(416 - 16)$	(f)
$Cu_{78.6}Sn_{21.4}$	17.980	$cF(416 - 4)$	(f)
$Cu_{79.8}Sn_{20.2}$	17.9646	$cF416$	(g)
Subtype I/II	(3 structures)	$cF(488 - d - x)$	
$Zn_{89.1}Ir_{10.9}$	18.224	$cF(452 - 36)$	(h)
$Zn_{90.5}Ir_{9.5}$	18.224	$cF(456 - 36)$	(h)
$Zn_{91.1}Ir_{8.9}$	18.214	$cF(456 - 35)$	(h)
Subtype II	(11 structures)	$cF(440 - x)$	
$Na_{86.3}Tl_{13.7}$	24.154	$cF408$	(i)
$Sc_{86.3}Os_{13.7}$	20.771	$cF408$	(j)
$Mg_{87.3}Ru_{12.7}$	20.19	$cF408$	(k)
$Mg_{86.3}Rh_{13.7}$	20.148	$cF408$	(l)
$Mg_{87.9}Ir_{12.1}$	20.1148	$cF396$	(m)
$Mg_{85.9}Pd_{14.1}$	20.105	$cF396$	(n)
$Mg_{86.3}Ir_{13.7}$	20.097	$cF408$	(o)
$Zn_{95.3}Mo_{4.7}$	18.464	$cF(420 - 23)$	(p)
$Al_{65.3}Cu_{18.1}Cr_{16.6}$	18.16	$cF(412 - 28)$	(q)
$Zn_{86.6}Fe_{6.7}Ni_{6.7}$	18.0838	$cF(416 - 1)$	(r)
$Zn_{78.4}Fe_{21.6}$	17.963	$cF408$	(s)
Subtype II′	(2 structures)	$cF(440 - x + a)$	
$In_{54.5}Pd_{29.3}Ce_{16.3}$	21.81382	$cF492$	(t)
$Zn_{67.5}Ce_{16.7}Mg_{15.8}$	21.1979	$cF480$	(u)
Subtype III	(4 structures)	$cF(448 - x)$	
$Mg_{83.6}Gd_{16.4}$	22.344	$cF(448 - 4)$	(v)
$Cd_{80.4}Sm_{19.6}$	21.699	$cF448$	(w)†
$Al_{63.6}Ta_{36.4}$	19.153	$cF444$	(x), (y)
$Mg_{82.4}Y_{9.0}Ce_{8.6}$	17.1833	$cF(448 - 8)$	(z)
Subtype III′	(1 structure)	$cF(448 - x + a)$	
$Na_{49.2}Ba_{28.8}Li_{22.0}$	27.335	$cF472$	(aa)
Subtype IV	(1 structure)	$cF(456 - x)$	
$Na_{49.1}Sn_{26.3}In_{24.6}$	22.993	$cF456$	(bb)
$F\bar{4}3m$, $(4 \times 4 \times 4)$-fold superstructure (1), $cF(1124 - x)$			
$Cu_{56.9}Cd_{43.1}$	25.871	$cF1124$	(cc)
$F\bar{4}3m$, $(7 \times 7 \times 7)$-fold superstructure (1), $cF(5928 - x)$			
$Al_{56.6}Ta_{39.5}Cu_{3.9}$	45.376	$cF(5928 - 20)$	(x)
$F\bar{4}3m$, $(11 \times 11 \times 11)$-fold superstructure (1), $cF(23\,256 - x)$			
$Al_{55.4}Ta_{39.1}Cu_{5.4}$	71.490	$cF(23\,256 - 122)$	(x
$Fd\bar{3}m$, $(3 \times 3 \times 3)$-fold superstructures (7), $cF464$			
$In_{70.7}K_{29.3}$	24.241	$cF464$	(dd)
$Ga_{50.0}Na_{29.3}In_{20.7}$	21.785	$cF464$	(ee)
$Ga_{48.9}Na_{30.4}Cd_{20.7}$	21.286	$cF(464 - 4)$	(ff)
$Ga_{63.0}Na_{31.0}Ag_{6.0}$	20.857	$cF464$	(gg)
$Ga_{53.4}Li_{31.0}Cu_{8.6}In_{6.9}$	19.928	$cF464$	(hh)
$Ga_{47.5}Mg_{31.2}Cu_{21.3}$	19.8742	$cF(464 - 13)$	(ii)

Table 1 (continued)

Composition	a (°A)	Pearson	Reference
$Zn_{61.0}Ca_{35.6}Ni_{3.4}$	21.5051	$cF472$	(jj)
$Fd\bar{3}m$, $(4 \times 4 \times 4)$-fold superstructures (2), $cF(1192 - x)$			
$Al_{53.6}Mg_{46.4}$	28.239	$cF(1192 - 23)$	(kk)
$Cd_{66.7}Na_{33.3}$	30.56	$cF(1192 - 40)$	(ll)
$Fd\bar{3}$, $(4 \times 4 \times 4)$-fold superstructure (1), $cF1392$			
$Cd_{86.2}Eu_{13.8}$	31.8718	$cF1392$	(mm)
$Fm\bar{3}m$, $(4 \times 4 \times 4)$-fold superstructures (4), $cF(1208 - x)$			
$Pr_{40.9}Sn_{39.2}Co_{19.9}$	30.8202	$cF(1208 - 64)$	(nn)
$Dy_{40.9}Sn_{39.2}Co_{19.9}$	29.831	$cF(1208 - 64)$	(oo)
$Gd_{41.6}Ge_{39.9}Fe_{18.5}$	28.7680	$cF1124$	(pp)
$Tb_{41.6}Ge_{39.9}Fe_{18.5}$	28.580	$cF1124$	(qq)
$Fm\bar{3}c$, $(4 \times 4 \times 4)$-fold superstructures (3), $cF(992 - x)$			
$Zn_{67.1}Sn_{20.8}Mo_{12.1}$	25.447	$cF(944 - 21)$	(rr)
$Zn_{57.3}Ru_{22.2}Sb_{20.5}$	25.098	$cF(968 - 32)$	(ss)
$Zn_{76.9}Ru_{12.0}Sb_{11.1}$	24.355	$cF(992 - 125)$	(ss)

References: (a) Pavlyuk et al. (2007), (b) Goward et al. (2001), (c) Thimmaiah & Miller (2010), (d) Thimmaiah et al. (2003), (e) Johansson & Westman (1970), (f) Booth et al. (1977), (g) Arnberg et al. (1976), (h) Hornfeck et al. (2004), (i) Samson & Hansen (1972), (j) Chabot et al. (1980), (k) Westin & Edshammar (1973), (l) Westin & Edshammar (1971), (m) Bonhomme & Yvon (1995), (n) Samson (1972), (o) Westin & Edshammar (1972), (p) Nasch & Jeitschko (1999), (q) Sugiyama et al. (2002), (r) Lidin et al. (1994), (s) Koster & Schoone (1981), (t) Tursina et al. (2005), (u) Pavlyuk et al. (2008), (v) Fornasini et al. (1986), (w) Fornasini et al. (1978), (x) Weber et al. (2009), (y) Mahne & Harbrecht (1994), (z) Gribanov et al. (1993), (aa) Smetana et al. (2006), (bb) Blase et al. (1991), (cc) Samson (1967), (dd) Cordier & Müller (1993a), (ee) Cordier & Müller (1993b), (ff) Tillard-Charbonnel & Belin (1992), (gg) Tillard-Charbonnel et al. (1993), (hh) Chahine et al. (1995), (ii) Lin & Corbett (2005), (jj) Stojanovic & Latturner (2007), (kk) Samson (1962), (ll) Samson (1965), (mm) Gómez & Lidin (2004), (nn) He et al. (2010), (oo) Salamakha et al. (2001), (pp) He et al. (2007), (qq) Pecharskii et al. (1987), (rr) Hillebrecht et al. (1997), (ss) Xiong et al. (2010). † This report also mentions that isostructural $Cd_{80.4}RE_{19.6}$ compounds were found with RE = Y, Pr, Nd, Gd, Tb, Dy, Ho, Er, Tm, Lu rather than Sm.

chemical properties. They range from Zintl phases to transition metal aluminides, from alkali-metal/alkaline-earth metal compounds to ones just between transition metals. Consequently, since their crystal structures are similar they are dominated by geometrical packing principles rather than by the significantly differing chemical bonding or electronic interactions.

A short comment on preferred space-group symmetries: the point symmetry of a cluster centered at a given Wyckoff position is that of this special site; of course, the symmetry of a cluster is controlled by the most energetically favorable atomic arrangement under the constraint of optimum cluster packing and not by the Wyckoff symmetry of the space group. The symmetry of a cluster determines the type of Wyckoff position it can be described with and constrains the number of possible space groups characterizing its packing. In other words, the space-group symmetry of a structure is a consequence, and not the origin of the best possible packing of atoms, AETs or clusters under the constraint of free-energy minimization.

In the case of the most frequent space-group symmetries among the structures we chose for examination $F\bar{4}3m$ and $Fd\bar{3}m$, the AETs most useful for the structural description will be tetrahedra (t) and truncated tetrahedra (tt) decorated with atoms, AETs or clusters. Only a single packing of uniform polyhedra exists that shows global tetrahedral symmetry,

feature articles

$Fd\bar{3}m$, which is just a packing of these two types of regular polyhedra.

2.1. Packings of tetrahedra, truncated tetrahedra and endohedral clusters

The tt is one of the AETs constituting the Frank–Kasper (FK) phases. In most cases the tt are centered by one type of atom, A, while all 12 vertices are occupied by another type, B; four more atoms of type A cap the h(exagon) faces of the tt. This gives a total coordination number (CN) of 16 for the central A atom. Therefore, this AET is usually termed CN16 FK polyhedron or Friauf polyhedron FK_{16}^{28}. Hereafter Frank–Kasper polyhedra will be expressed by FK_V^F if they exhibit F triangle faces and V vertices. The size of the tt is determined by the distance $d_{B-B} = a$ between B atoms, where a is the edge length of the tt; $d_{A-A} = a\sqrt{6}/2 \simeq 1.22474a$ and $d_{A-B} = a\sqrt{22}/4 \simeq 1.17260a$. In case types A and B atoms correspond to hard spheres with radii $a\sqrt{6}/4 \simeq 0.61237a$ and $a/2$; all atoms would only touch atoms of the same type. Consequently, Friauf polyhedra are energetically more favorable if attractive $A-A$ and $B-B$ interactions are stronger than $A-B$ interactions. The ideal ratio of the atomic radii corresponds to $r_A/r_B = \sqrt{3/2}$. The difference between d_{A-B} and the summed-up radii of atoms A and B is $0.06023a$, which would be the gap width in the case of equally sized hard spheres. In an atomic arrangement this gives the tt some flexibility to distort and allows for a large variety of packings.

Layers of tt/t can be stacked to give cubic or hexagonal structures with the general composition AB_2 such as the Laves phases $cF24$-MgCu$_2$, $hP16$-MgZn$_2$ and $hP24$-MgNi$_2$. A different stoichiometry results from three-dimensional frameworks or spherical clusters of tt/t (e.g. the Samson cluster). While tetrahedral symmetry prevails in the first case, pentagonal arrangements are typical for the second. The outer shell of B atoms forms fullerene-like structures (fullerenes, for short) F_V^F with 12 p(entagon) faces plus H h faces ($F = 12 + H$) and $V = 20 + 2H$ vertices. H equals the number of Friauf polyhedra constituting the cluster shell. The outer A atoms form generalized FK polyhedra FK_V^F with V faces and F vertices (deltahedra, covered by only triangular faces with either five- or sixfold vertex symmetry; Alvarez, 2005, 2006). The inner cluster shell formed by the triangle faces of the Friauf polyhedra is a FK polyhedron with H faces.

2.2. Superstructure description

All the complex intermetallic structures discussed in this work can be regarded as ($p \times p \times p$)-fold (or p^3-fold) super-structures of a basic structure ($p = 3, 4, 7, 11$). The easiest way to recognize a smaller unit underlying the periodic cell is by evaluating the diffraction pattern with respect to the strongest reflections. This is obvious from the calculated diffraction patterns as they are shown in Fig. 2 for the mentioned superstructures and possible basic structures (see below). Therein, the strongest reflections of structures considered as

being p^3-fold superstructures with $p = 3, 4, 7, 11$ bear the indices 6 6 0, 8 8 0, 14 14 0 and 22 22 0, corresponding to face-centered unit cells of the respective metric.
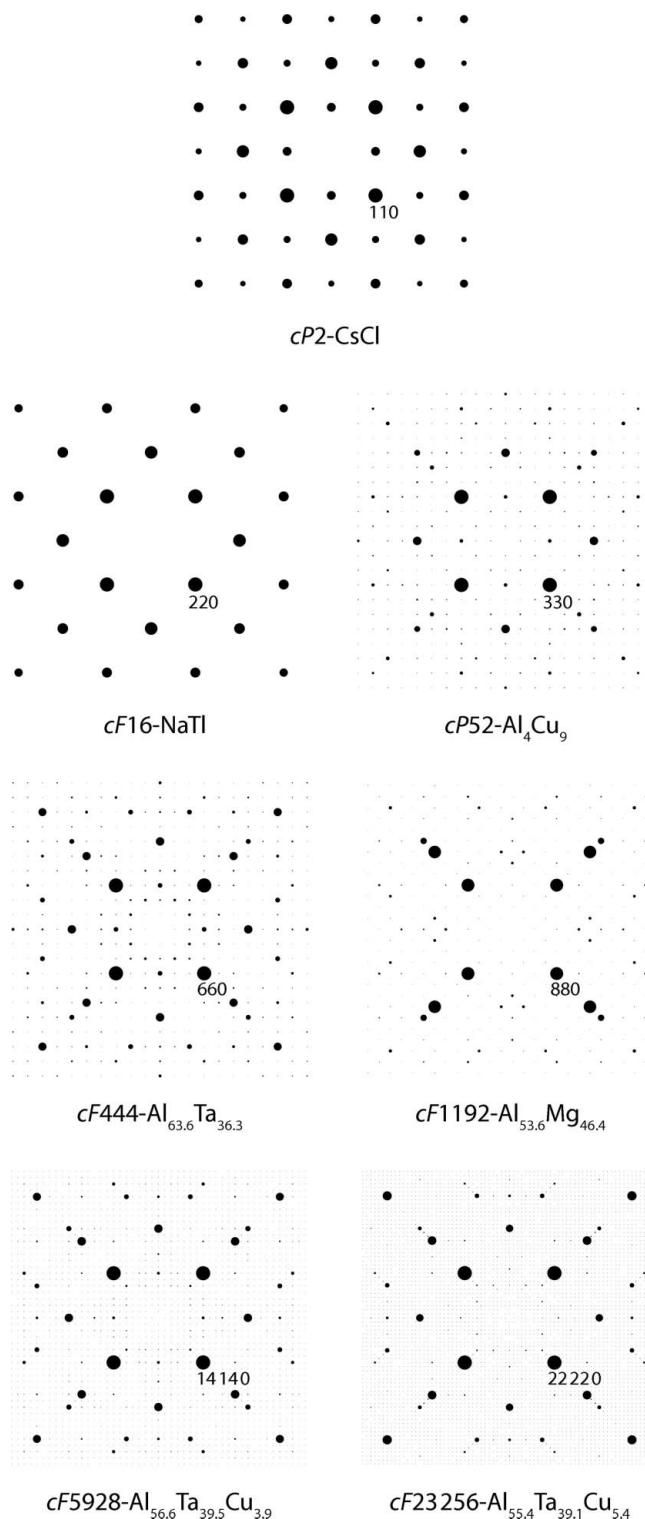

Figure 2
$hk0$ plane of the diffraction pattern as simulated for Al$_{63.6}$Ta$_{36.4}$, Al$_{53.6}$Mg$_{46.4}$, Al$_{56.6}$Ta$_{39.5}$Cu$_{3.9}$, Al$_{55.4}$Ta$_{39.1}$Cu$_{5.4}$, as well as three structure types, which can be regarded as potential corresponding basic structures (CsCl, NaTl and Al$_4$Cu$_9$). The most intense reflections are labelled by their indices – they coincide for all the structures shown.
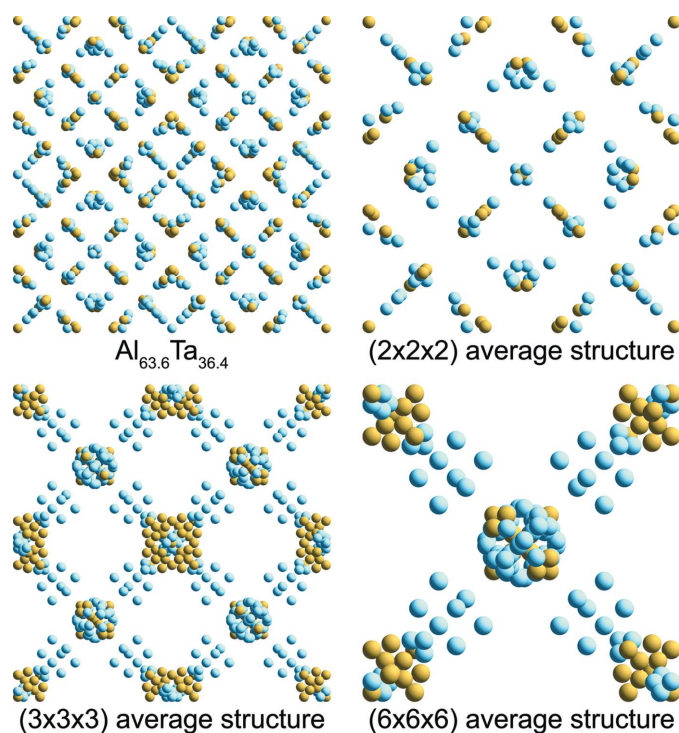
Figure 3
Unit cell and different average structures of $cF464$ intermetallics, shown using the example of $Al_{63.6}Ta_{36.4}$. The average structures shown correspond to the assumption of $(2 \times 2 \times 2)$-, $(3 \times 3 \times 3)$- and $(6 \times 6 \times 6)$-fold superstructures. The unit-cell parameters are approximately 19.2 Å for the original unit cell and 9.6, 6.4 and 3.2 Å for the respective average structures. The underlying basic structures are of the γ-brass-, NaTl- and CsCl-type.

The fact that the compounds investigated are superstructures can be easily visualized by their distinct average structures, as shown in the respective sections (§§3.1, 3.3, 4 and 5). The average structure of a superstructure results if it is projected into one unit cell of the basic structure. Previously the $cF \simeq 400$ structures were usually discussed as $(2 \times 2 \times 2)$-fold superstructures of the γ-brass structure type, $cI52$-Cu_5Zn_8 (Johansson & Westman, 1970; Arnberg *et al.*, 1976; Booth *et al.*, 1977; Fornasini *et al.*, 1978; Lidin *et al.*, 1994; Thimmaiah *et al.*, 2003; Berger *et al.*, 2008). This structural relationship seemed obvious since the structures also feature 26-atom groups that were previously identified as constituents of γ-brasses. On the other hand, the γ-brass structure itself can be considered as already being a $(3 \times 3 \times 3)$-fold superstructure of the $cP2$-CsCl structure type, with two sites of this supercell vacant. Accordingly, the structures with $p = 3$ ($cF \simeq 400$) can also be regarded as $(6 \times 6 \times 6)$-fold superstructures of the $cP2$-CsCl type.

Using the example of $cF444$-$Al_{63.6}Ta_{36.4}$ Fig. 3 shows the unit cell as well as the different average structures projected along [001]. The corresponding basic structures have space-group symmetries $P\bar{4}3m$ (2^3-fold superstructure of $cP52$-P-cell-γ-brass), $F\bar{4}3m$ (3^3-fold superstructure of a $cF16$-NaTl derivative) or $Pm\bar{3}m$ (6^3-fold superstructure of a $cP2$-CsCl-type structure). The symmetry relations can be directly read

from the diagram in Fig. 4. They are also listed in detail in Section 1 of the supplementary material.[3] Accordingly, the indices of the group–subgroup relations are easily determined as 2, 27 and 108.

Using the $cF16$ unit cell for the basic structure we not only preserve the maximum point symmetry ($\bar{4}3m$) but also the centering. Alternatively, the CsCl structure type may be used, however, involving the loss of F-centering. The γ-brass structure does not appear to be the ideal choice for a simple reason: the superstructures with $p = 8, 14, 22$ with regard to the $cP2$-CsCl-type cannot be described as superstructures of γ-brass, which itself is a $(p = 3)$-fold superstructure of $cP2$-CsCl. Hence we choose the $cF16$-NaTl structure type as the basic structure for a unifying description with maximum symmetry.

As mentioned before, another indication of an underlying basic structure is based on the intensity distribution of the diffraction patterns: the reciprocal lattice of a superstructure features a subset of strong reflections related to the average structure along with a much larger number of weak reflections caused by deviations from the basic structure. Fig. 2 shows the calculated diffraction patterns of representative structures for all unit-cell dimensions discussed here.[4] Obviously, the reflections of highest intensity are the same for all structures. Their indices are also given in the graph and increase with increasing unit-cell size, while the sets of net planes they refer to remain the same. Consequently, all the structures discussed here can be regarded as superstructures of a $cF16$-NaTl-like cell. In principle, they can also be regarded as superstructures of $cP2$-CsCl (the same is true for $cF16$-NaTl and γ-brass-type structures).

2.3. Basic structures

The basic structures of all the cubic compounds discussed here are of the $cF16$-NaTl structure type ($Fd\bar{3}m$) or of one of its derivatives with lower symmetry. The details and symmetry of these basic structures are given in Section 1 of the supplementary material.

For the $p = 3$ superstructures with space groups $F\bar{4}3m$ and $Fd\bar{3}m$ the symmetries of the basic structures with the $cF16$ unit cell are the same as for the respective superstructures.

The basic structures of the $p = 4$ superstructures are of the type $cP16$, geometrically similar to the previously discussed $cF16$-NaTl structure type but with different site relationships. The average structure of $cF1124$-$Cu_{56.9}Cd_{43.1}$ ($F\bar{4}3m$), with space group $P\bar{4}3m$, looks more scattered in comparison to the $p = 3$ ones. The average structures of $cF(1192 - 40)$-$Cd_{66.7}Na_{33.3}$ and $cF(1192 - 23)$-$Al_{53.6}Mg_{46.4}$ ($Fd\bar{3}m$) look similar to that of $cF1124$-$Cu_{56.9}Cd_{43.1}$ and also exhibit a reduction in lattice symmetry, but in this case to space group $Pm\bar{3}m$. The same is true for the $p = 4$ superstructures in space groups $Fm\bar{3}m$ and $Fm\bar{3}c$ such as $cF(944 - 22)$-
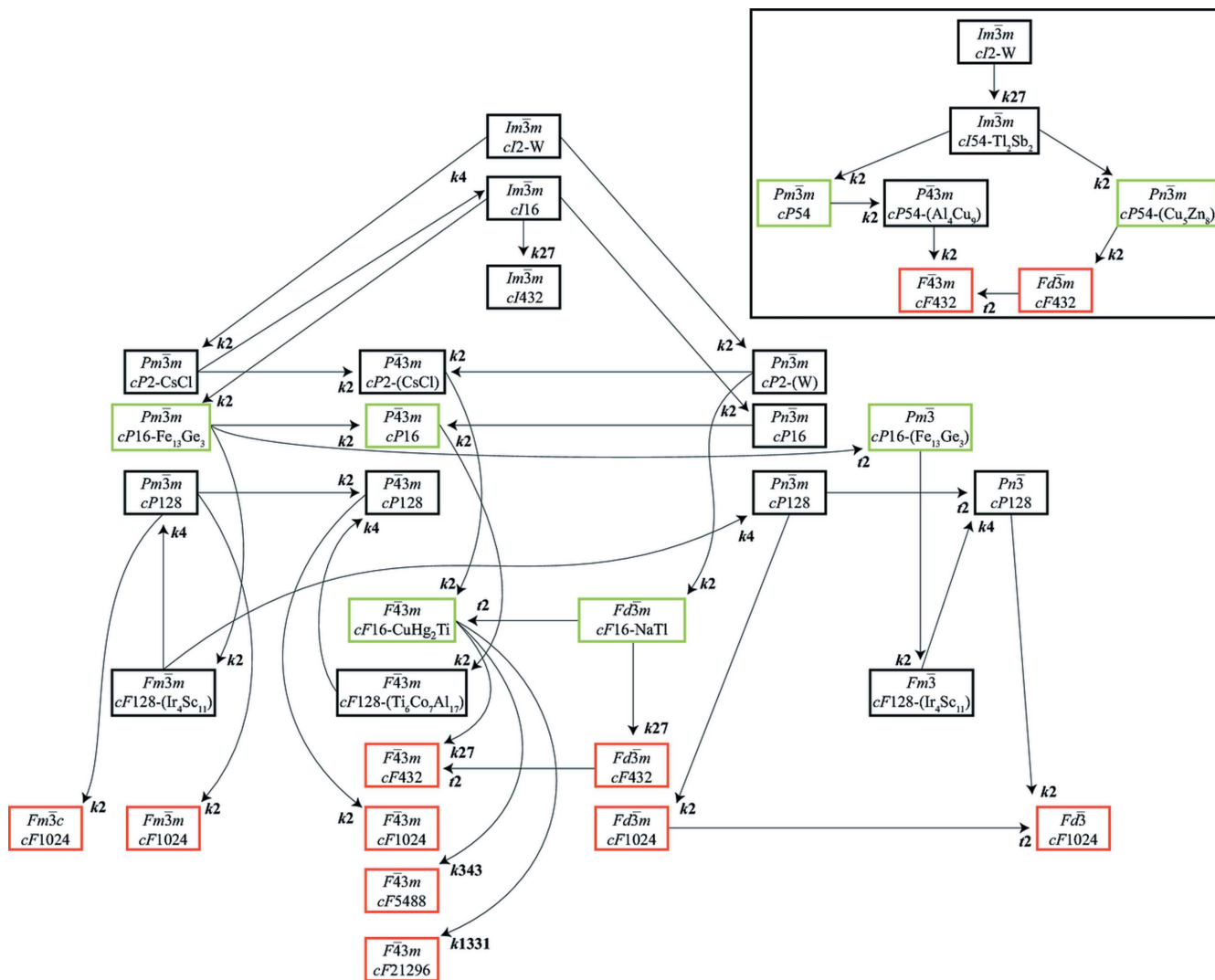
Figure 4
Bärnighausen-like symmetry overview for f.c.c. intermetallics and their average structures. Given are the respective space groups, Pearson symbols as well as structure types (if any). Structure types in parentheses belong to the same lattice complex but a different space group or differ slightly with respect to atomic sites (*e.g.* with one site unoccupied). All arrows point from the super- to the respective subgroup and are marked with *t* for *translationengleiche* and *k* for *klassengleiche* subgroups as well as the index of the relation. The structures covered in this work are marked in red and the basic structures discussed are marked in green.

$Zn_{67.1}Sn_{20.8}Mo_{12.1}$. The basic structure of the superstructures with symmetry $Fd\bar{3}$ can be described in the space group $Pm\bar{3}$, which is a *translationengleiche* subgroup of $Pm\bar{3}m$.

Fig. 4 illustrates the group–subgroup relations between all relevant space groups of the f.c.c. complex intermetallics and their average (and basic) structures. Each prototype structure is represented by its space group, Pearson symbol and – if available – the name of the structure type, a representative or a very similar structure. Direct symmetry transitions are shown by arrows, pointing from super- to subgroup and bearing a symbol which expresses the type of subgroup – *t* for *translationengleiche* and *k* for *klassengleiche* – as well as its index.

The symmetry graph starts with the $cI2$-W structure type ($Im\bar{3}m$). The average structure types discussed above are derived *via* the $cP2$-CsCl type and other intermediate structures. They exhibit space groups $Pm\bar{3}m$, $P\bar{4}3m$ and $Pm\bar{3}$ in the

case of ($p = 4$)-superstructures ($cP16$) and space groups $F\bar{4}3m$ and $Fd\bar{3}m$ for the other compounds ($cF16$). The space groups of the average structures are marked in green and the superstructure space groups in red in Fig. 4. The structure types found to be related to the displayed prototype structures are given in Table 2 of the supplementary material. The atomic sites in the different space groups and their interrelations are given in Tables 3–17 of the supplementary material.

2.4. Fundamental sets of atomic layers and the superstructure concept

All crystal structures in thermodynamic equilibrium show n-dimensional lattice symmetry, with $n = 3$ for regular crystals and $n > 3$ for aperiodic crystals such as quasicrystals or incommensurate crystals.

Table 2
Atomic sites of the cubic complex intermetallics discussed here in space group $F\bar{4}3m$.

The Wyckoff site is included in the site label. The subtypes, which feature the respective sites, are given.

Site	Symmetry	$\bar{x}(\sigma)$	$\bar{y}(\sigma)$	$\bar{z}(\sigma)$	Idealized coordinates	Subtypes
16e1	.3m	0.165 (6)	x	x	1/6 1/6 1/6	All
16e2	.3m	0.418 (10)	x	x	5/12 5/12 5/12	All
16e3	.3m	0.660 (13)	x	x	2/3 2/3 2/3	All
16e4	.3m	0.915 (5)	x	x	11/12 11/12 11/12	All
48h1	..m	0.157 (6)	x	0.019 (8)	1/6 1/6 1/48	All
48h2	..m	0.091 (9)	x	0.269 (9)	1/12 1/12 13/48	All
48h3	..m	0.176 (17)	x	0.517 (6)	1/6 1/6 25/48	All
48h4	..m	0.097 (12)	x	0.773 (10)	1/12 1/12 37/48	All
4a	$\bar{4}3m$	0	0	0	0 0 0	(All)
4b	$\bar{4}3m$	0.5	0.5	0.5	1/2 1/2 1/2	(All)
4c	$\bar{4}3m$	0.25	0.25	0.25	1/4 1/4 1/4	(All)
4d	$\bar{4}3m$	0.75	0.75	0.75	3/4 3/4 3/4	(All)
16e5	.3m	0.059 (11)	x	x	3/48 3/48 3/48	I, II, III, IV
16e6	.3m	0.311 (13)	x	x	15/48 15/48 15/48	I, II, III
16e7	.3m	0.561 (9)	x	x	27/48 27/48 27/48	I
16e8	.3m	0.811 (14)	x	x	39/48 39/48 39/48	I, (II)
24f1	2.mm	0.176 (12)	0	0	1/6 0 0	I, II, III, IV
24f2	2.mm	0.323 (3)	0	0	1/3 0 0	I
24g1	2.mm	0.084 (15)	0.25	0.25	1/12 1/4 1/4	I, II, III
24g2	2.mm	0.608 (35)	0.25	0.25	7/12 1/4 1/4	I, II
48h5	..m	0.205	x	0.389	5/24 5/24 19/48	IV
48h6	..m	0.048 (4)	x	0.653 (11)	1/24 1/24 31/48	II, III, IV
48h7	..m	0.204 (2)	x	0.892 (3)	5/24 5/24 43/48	III, IV

The topological decomposition of crystal structures into atomic layers parallel to low-indexed lattice planes frequently gives insight into the structural building principles.

It has already been pointed out by Samson (1964) that every special Wyckoff position (crystallographic orbit) of the space groups $F23$, $Fd\bar{3}$, $F432$, $F\bar{4}3m$ and $F\bar{4}3c$ places at least one point on the (110) plane, which he named the 'most useful plane' for structure analysis. With some restrictions, this is also true for the cubic space groups $F4_{1}32$, $Fd\bar{3}m$ and $Fd\bar{3}c$.[5]

In the projected structures a clear layer structure can be seen. There are $2p$ (110) layers per period. For $p = 3$, for instance, one flat layer, located on a mirror plane, is sandwiched between two puckered layers. Each adjacent pair of such three-layer stacks ($3S$) is related by a glide plane yielding the stacking sequence $3S$–$3S'$–$3S$–$3S'$ along [110], with $3S'$ representing the three-layer stack symmetrically equivalent to $3S$.

Since the set of {110} layers consists of a framework of six, mutually intersecting, symmetrically equivalent layers, there are not so many degrees of freedom left for decorating the layers properly, i.e. with reasonable atomic distances. In the case of an energetically favorable formation of particular AETs and larger clusters, additional constraints are imposed. The unit-cell dimensions of the discussed complex inter-

metallic phases are controlled by the number of layers, which in turn depends on the cluster size and their way of packing.

In the case of layer structures, we can expect the existence of average structures. In other words, the actual structures can be seen as superstructures or modulated structures. In the case at hand, the underlying basic structure common to all structures is related to a type of double-diamond structure. Taking the actual structure modulo the unit cell of the basic structure gives the average structure. Thereby each three-layer stack is projected into a single flat layer located on a mirror plane. This superstructure approach is obvious in reciprocal space. There the Bragg reflections with indices hkl and $h, k, l = 3n$ have particularly high intensities (Fig. 2, see §2.3).

In the case of some structures with $p = 4$, the {100} layers are also quite important. In the case of space group $Fd\bar{3}c$ the {110} layers are no longer relevant, only the {100} ones (as can be seen in §5.2). This structure can certainly be seen as cluster-dominated, which is also reflected in the average structure.

3. Structures with space-group symmetry $F\bar{4}3m$

Of the 39 complex intermetallics crystallizing in the space group $F\bar{4}3m$, all but three can be regarded as $(3 \times 3 \times 3)$-fold superstructures of a double-diamond-type basic structure with unit-cell parameters similar to those of the (fictitious) cubic Laves phase in the respective system. The others, $cF1124$-$Cu_{56.9}Cd_{43.1}$ (Samson, 1967), $cF(5928 - 20)$-$Al_{56.6}Cu_{3.9}Ta_{39.5}$ and $cF(23256 - 122)$-$Al_{55.4}Cu_{5.4}Ta_{39.1}$ (Weber et al., 2009; Conrad et al., 2009), correspond to p^3-fold superstructures with $p = 4$, 7 and 11.

For the 36 structures with $p = 3$, certain similarities – of chemical as well as purely geometrical type – become apparent immediately. Since they share a considerable amount of common atomic sites, they can be grouped into four different subtypes of one aristotype (Table 1). In Fig. 5 the projected unit cells are shown for one representative of each subtype together with its average structure. The atomic coordinates of an average structure can be obtained by taking all atomic coordinates modulo the unit cell of the basic structure: $(x_{av}, y_{av}, z_{av}) = (px, py, pz)$ mod (1). The basic structure in turn is related to $cF16$-NaTl.[6]

In Table 1 the Pearson symbols for the different structural subtypes are shown with the number of atoms for fully occupied atomic sites minus x, the total number of missing atoms [e.g. $cF(432 - x)$]. In the case of partially occupied sites, on average x need not be an integer. For the mixed subtypes I/II the set union is given and part of the sites are bound to be unoccupied in order to produce a physically valid structure. The variants II′ and III′ include additional sites increasing the number of atoms per unit cell.

---

[5] Within the scope of this work only the face-centered space groups are listed. These considerations also hold true for $P2_{1}3$ and $Pa\bar{3}$, and with minor restrictions for $P4_{3}32$ and $P4_{1}32$.

[6] It can also be seen as the structure of $cF24$-$MgCu_2$ with the additionally occupied Wyckoff position $8b$ $\frac{1}{2}, \frac{1}{2}, \frac{1}{2}$.
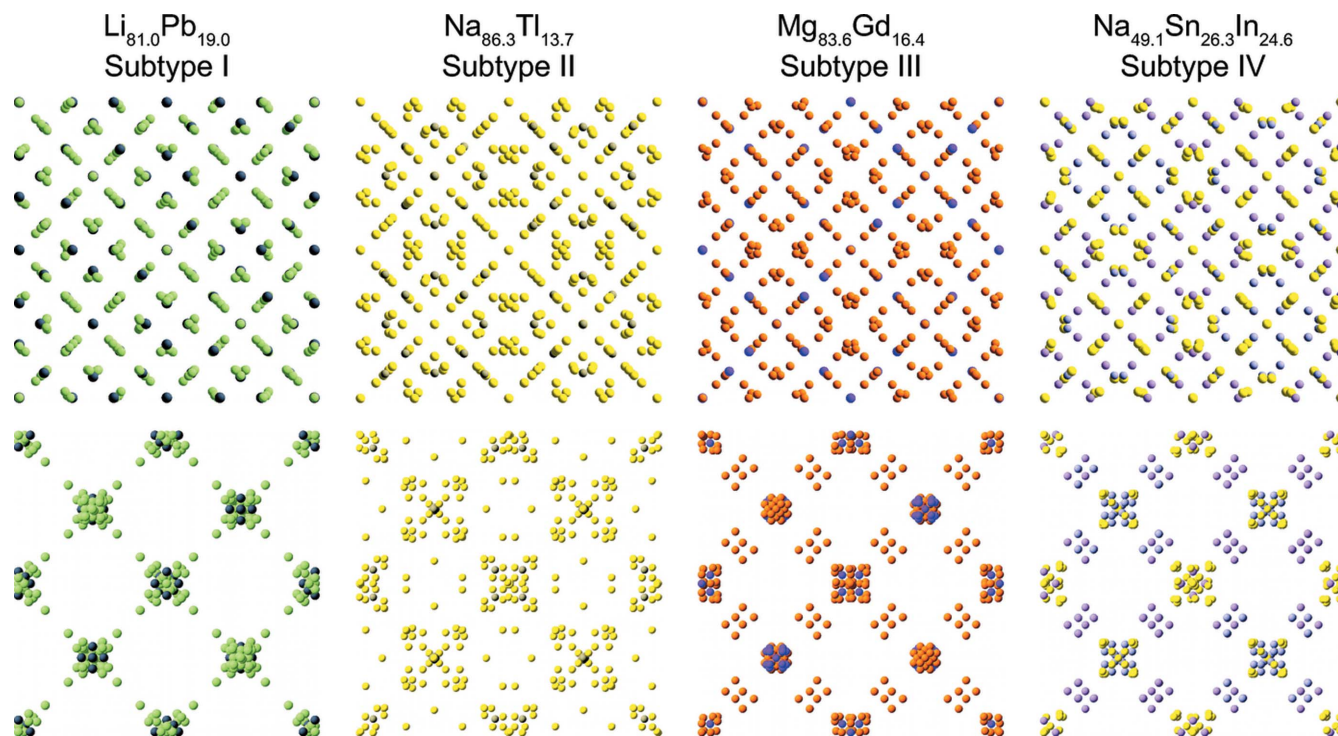
Figure 5
Unit cells of the different subtypes of the $cF \simeq 400$ complex intermetallic structures in the space group $F\bar{4}3m$. The projection of the unit cell along the [001] direction (upper) and a similar projection of the respective average structure (lower) are shown. Here, representatives for the different subtypes are chosen.

3.1. $(3 \times 3 \times 3)$-fold superstructures – $cF(464 - x)$

The four subtypes of $(3 \times 3 \times 3)$-fold superstructures have in common a partial structure formed by a subset of eight atomic sites (see upper part of Table 2). The rather small standard deviations of the averaged atomic coordinates (obtained by averaging the respective coordinates of all 36 structures with symmetry $F\bar{4}3m$) indicate that these four structures are quite similar variants of one and the same aristotype. There are only small differences in the occupancies and/or the way of splitting some sites. The sites whose occupations differ among the different structural subtypes are given in the lower part of Table 2.

Consequently, all representatives of the $(3 \times 3 \times 3)$-fold superstructure class show a cluster structure similar to that of $cF444$-$Al_{63.6}Ta_{36.4}$ (Conrad *et al.*, 2009), which can be seen as cubic close packing of three-shell clusters with the shape of a F_{76}^{40} fullerene (with 40 faces and 76 vertices) and tetrahedral symmetry. These clusters share their 12 *p* faces with their neighbors. The second cluster shell is formed by a FK_{40}^{76} polyhedron (76 triangle faces and 40 vertices) dual to the fullerene shell.[7] The first (innermost) shell corresponds either to a CN14 rhombic dodecahedron or a CN16 Friauf polyhedron (Fig. 6), which are centered by an atom in some structures and in others are not.

This main cluster is centered at one of the four points of highest symmetry, $\bar{4}3m$, in space group $F\bar{4}3m$, *i.e.* the Wyckoff

positions $4a$ $0, 0, 0$, $4b$ $\frac{1}{2}, \frac{1}{2}, \frac{1}{2}$, $4c$ $\frac{1}{4}, \frac{1}{4}, \frac{1}{4}$ or $4d$ $\frac{3}{4}, \frac{3}{4}, \frac{3}{4}$. They are essentially interchangeable, as the space-group symmetry is invariant with respect to origin shifts of $+\left(\frac{1}{4}, \frac{1}{4}, \frac{1}{4}\right)$, $+\left(\frac{1}{2}, \frac{1}{2}, \frac{1}{2}\right)$ or $+\left(\frac{3}{4}, \frac{3}{4}, \frac{3}{4}\right)$. With this in mind, all these sites are equally considered as centers of significant clusters.

3.1.1. First cluster shell. The aristotype structure corresponds to the union of the different subtypes. Subtype I contains only rhombic dodecahedra (*rd*) around the points of highest symmetry, subtype II three rhombic dodecahedra and one Friauf polyhedron (*F*), subtype III two of each kind and subtype IV three Friauf polyhedra and only one rhombic dodecahedron. The arrangement of these first-shell clusters along the body diagonal of the unit cell – at $0, 0, 0$; $\frac{1}{4}, \frac{1}{4}, \frac{1}{4}$; $\frac{1}{2}, \frac{1}{2}, \frac{1}{2}$; $\frac{3}{4}, \frac{3}{4}, \frac{3}{4}$ – is the following:

Subtype I – *rd rd rd rd*,
Subtype II – *rd rd F rd*,
Subtype III – *rd rd F F*,
Subtype IV – *rd F F F*.

In the actual structures reduced *rd* forms are also observed when some sites remain unoccupied, resulting in either an octahedron with only half of its faces capped or a cube. Some structures between the subtypes are also found, $Zn_{89.1}Ir_{10.9}$, $Zn_{90.5}Ir_{9.5}$ and $Zn_{91.1}Ir_{8.9}$, which exhibit a partially occupied Friauf polyhedron and a rhombic dodecahedron centered on the same site. Corresponding to the often disordered first cluster shells, the positions of the central atoms are disordered in numerous cases.

3.1.2. Second cluster shell. The second cluster shell has the same shape in all subtypes of the aristotype: the FK_{40}^{76} poly-

---

[7] A dual polyhedron corresponds to the original one by replacing faces by vertices and *vice versa*. The dual of a dual is the original polyhedron.

hedron is found for all structures at sites $4a$–$4d$. The corresponding atomic positions build the skeletal structure which is common to all $cF464$ structures in the space group $F\bar{4}3m$.

3.1.3. Third cluster shell. Contrary to the second cluster shell, the third shell varies in shape from subtype to subtype.

All different versions, as well as their respective types of faces (triangles t, quadrangles q, pentagons p and hexagons h) are given in Fig. 6.

In subtype I the third cluster shell is the same for all alternative sites ($4a$–$4d$): a 58-vertex polyhedron. The third-shell polyhedra go through a series of changes with evolving structural subtypes, as shown in Fig. 6. (The exact changes of the third-shell cluster throughout the different subtypes are listed in Table 20 of the supplementary material.) The noticeable F_{76}^{40} fullerene-like polyhedron is found on position $4c$ in subtypes III and IV.

The sites forming the different cluster shells are given in Table 18 of the supplementary material. Also given are their occupations for all discussed compounds in Tables 24 and 25 of the supplementary material.

3.2. Comment on the definition of cluster types

In connection with the description of the $cF(464 - x)$ structures as superstructures of the γ-brass structure type (see above), the atomic sites closest to the four Wyckoff positions $4a$–$4d$ were directly referred to as 'clusters'. Their packing was evaluated and their substructure divided into simpler polyhedra, directly apparent from the respective site symmetries (Johansson & Westman, 1970; Arnberg *et al.*, 1976; Booth *et al.*, 1977; Fornasini *et al.*, 1978; Chabot *et al.*, 1980; Fornasini *et al.*, 1986; Thimmaiah *et al.*, 2003; Hornfeck *et al.*, 2004). In this approach the atomic distances in the outer 'shells' become much larger than the sum of the atomic radii. In our cluster description, on the contrary, we only allow for polyhedra with edge lengths in the range of atomic interactions close to nearest-neighbor distances in the compound.

For comparing clusters, identifying different cluster shells and evaluating their spacing and their thickness/sphericity, a histogram of the interatomic distances can be
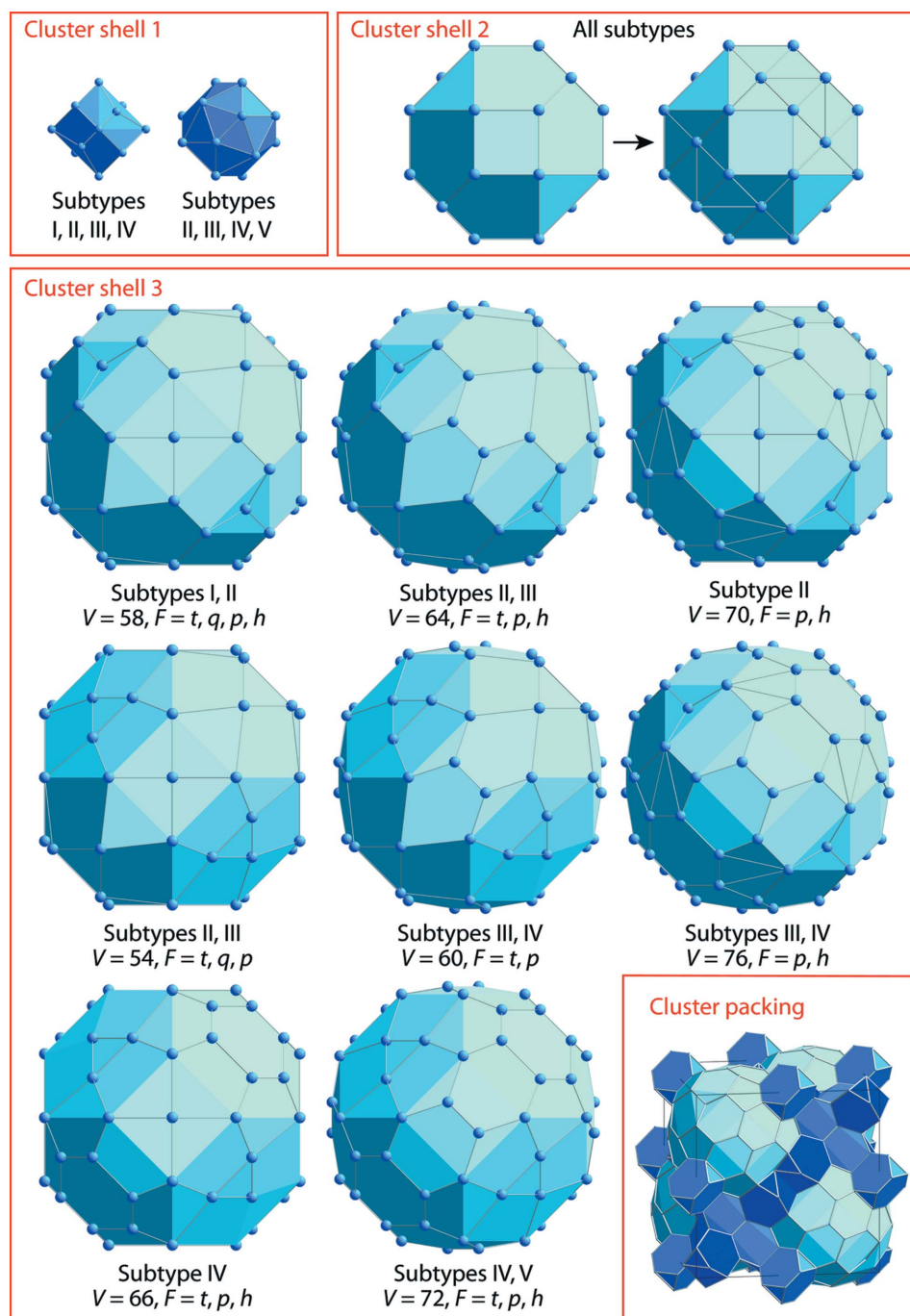

Figure 6
Main cluster of structures in space group $F\bar{4}3m$. The two variants of inner cluster shells are a (tetrahedrally distorted) rhombic dodecahedron and a Friauf polyhedron. The second cluster shell is in all cases a tetrahedrally truncated rhombic dodecahedron (truncated at all four- and half of the three-vertices) with atoms not only occupying corners, but also centering all pentagonal faces. The different third-shell clusters are designated with respect to their number of vertices V, types of faces F and the structural subtypes in which they occur. The packing of three-shell clusters in the unit cell is shown using the example of the F_{76}^{40} polyhedron – it is an f.c.c. packing.

quite useful. The number of atoms constituting the cluster shells must increase quadratically with the radius to keep their density constant (and also atomic distances).

The analysis of the interatomic distances in $Al_{63.6}Ta_{36.4}$ shows that the separation of cluster shells becomes increas-
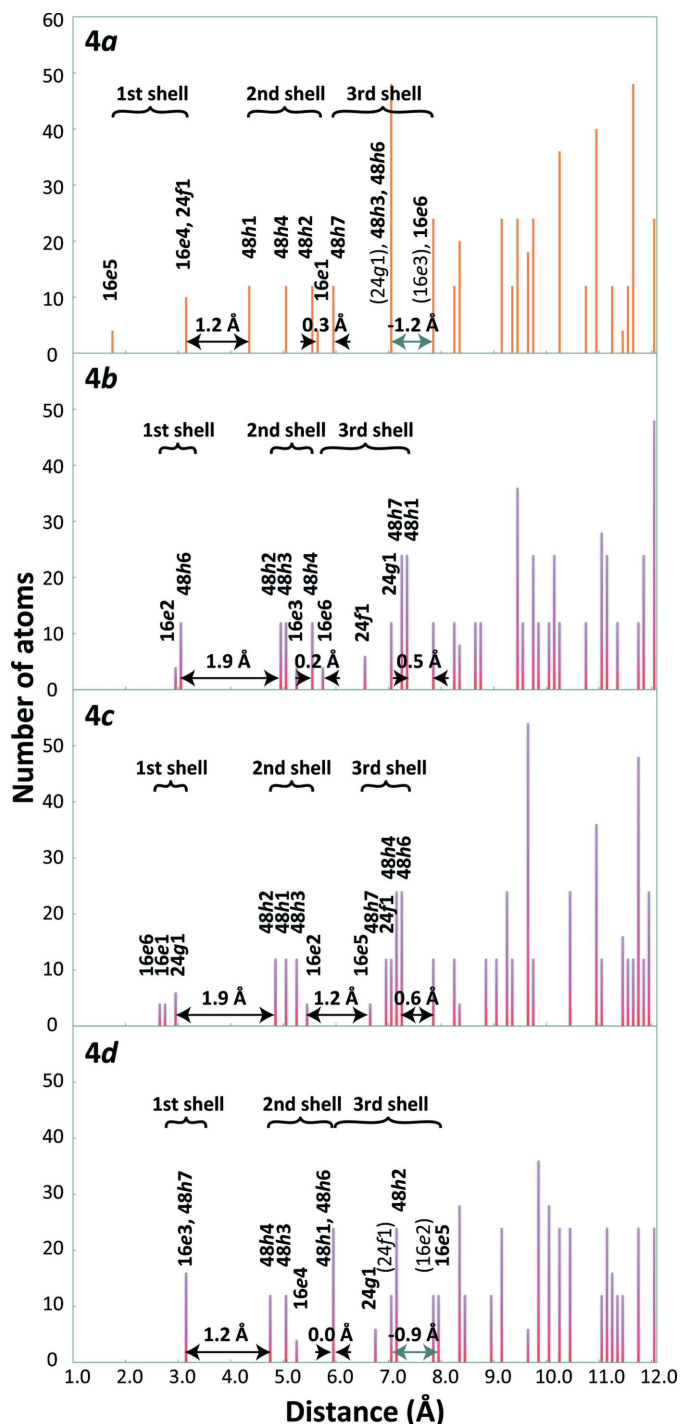
ingly difficult with increasing distances from the central atom. The first shell is quite easily recognizable around sites of all symmetries, while the definition of the second shell becomes quite ambiguous around low-symmetry sites. Fig. 7 shows the histograms corresponding to the highest symmetric atomic environments of sites 4b, 4c and 4d, as well as the unoccupied site 4a. In these diagrams the displayed atomic sites are specified, as well as the thicknesses of the three cluster shells around each of these positions. They can be separated to a different degree: the second and third shell at site 4d are not separated and around 4a and 4d the third shell is already overlapping with atomic sites belonging to the outer region. The best separation is found between the clusters at site 4c, which show larger distances between atoms of different cluster shells than the other ones. The distances between different shells are also larger than those within shells (which is not the case for the cluster around 4b) and, generally, the thickness of the shells is small. These findings support the kind of cluster description introduced by Conrad et al. (2009).

In general, it should be added that a cluster choice is in the first instance reasonable if the cluster shells chosen are as spherical as possible and well separated with respect to the distances between atoms in different cluster shells and the center of the nested clusters. Another important point is the occurrence of a certain cluster type: if clusters can be found independently in different structure types, this makes a good case for their significance. This type of more general cluster was for example found in the family of cubic Al–Cu–Ta compounds in the form of an Al_{76} fullerene-like cluster shell (Conrad et al., 2009).

3.3. Higher-order superstructures – cF1124, cF5928 and cF23256

The three largest intermetallic structures known in space group $F\bar{4}3m$ are $cF1124$-$Cu_{56.9}Cd_{43.1}$, $cF5928$-$Al_{56.6}Cu_{3.9}Ta_{39.5}$ and $cF23256$-$Al_{55.4}Cu_{5.4}Ta_{39.1}$, with lattice parameters of a around 25, 45 and 71 Å (Samson, 1967; Weber et al., 2009). Projections of the unit cells as well as of their average structures are shown in Fig. 8; for completeness, the structure of $cF444$-$Al_{63.6}Ta_{36.4}$ is also shown. In the superstructure description the structures are classified as $(3 \times 3 \times 3)$-, $(7 \times 7 \times 7)$- and $(11 \times 11 \times 11)$-fold superstructures of $cF16$-NaTl in the case of the Al-(Cu)-Ta compounds and as a $(4 \times 4 \times 4)$-fold one of an analogous $cP16$-type in the case of $cF1124$-$Cu_{56.9}Cd_{43.1}$.

3.3.1. Al–Cu–Ta structures. The close relationship between the three structures of the Al–Cu–Ta system is apparent: they are all superstructures of a double-diamond type basic structure with unit-cell parameters of the related cubic Laves phase. From a purely mathematical point of view, $(p \times p \times p)$-fold superstructures of a $F\bar{4}3m$ basic structure with the same symmetry can exist for all prime numbers $p>2$. The observed structures in the Al–Cu–Ta system, however, exhibit only three-, seven- and 11-fold supercells, e.g. fivefold supercells have not been found so far. This can be explained as follows.

Figure 7
Histogram of interatomic distances of atoms in the environment of the atomic sites 4a–4d in $Al_{63.6}Ta_{36.4}$ (Weber et al., 2009). These are the sites of highest symmetry in the space group ($F\bar{4}3m$) and therefore can bear the clusters of highest symmetry, as well as the biggest clusters without interpenetration. The 4c shell clearly shows the best-separated cluster shells.

The dominant feature in this group of structures is the endohedral cluster with the F_{76}^{40} third cluster shell. It is closely packed in the smallest structure ($p = 3$), whereas tetrahedrally assembled building blocks of four and ten such clusters are found in the medium and large structures with $p = 7$ and $p = 11$. These building blocks correspond to tetrahedra with edge lengths of two and three clusters. Therefore, it seems obvious that the three phases found are the only representatives of this family of structures and no intermediate superstructures can exist, although $p = 5$ would be equivalent from a group-theoretical perspective. On the other hand, superstructures with even bigger unit cells could be possible, at least geometrically.

3.3.2. $cF1124$-Cu$_{56.9}$Cd$_{43.1}$. The structure of $cF1124$-Cu$_{56.9}$Cd$_{43.1}$ has been reinvestigated several times after its first publication by Samson (1967). The structure was originally determined based on a 'packing map' of the structure – a cut through the structure along the (110) plane. It was described by two interpenetrating three-dimensional frameworks, composed of Friauf polyhedra and icosahedra, respectively, arranged in a diamond-like network (Samson, 1967). The Friauf network consists of tt sharing their hexagonal faces; the icosahedral network fits into its cavities and shares vertices with tt.

An alternative description interprets the structure in terms of octahedra and tetrahedra in addition to Friauf polyhedra (Andersson, 1980). That author also pointed out that complex phases like those discussed here are built up from structural features which are also found in simpler metallic structures. He also discusses that in the case of the Cu–Cd system the complex structure is packed more efficiently than the corresponding elementary metals and exhibits smaller interatomic distances. Both this description and the original one by Samson were analyzed later in conjunction with other complex structures explained as polyhedral frameworks by Hellner & Pearson (1987).

Kreiner & Schäpers (1997) pointed to the relationship between $cF1124$-Cu$_{56.9}$Cd$_{43.1}$ and the metastable icosahedral quasicrystal structure found in the Cd–Cu system with similar composition. The description as a hybrid structure by Samson (1967) is maintained, whereas the icosahedral network is explained in detail by means of the so-called $I3$-cluster concept. They identified the periodic structure to be an approximant structure of the quasicrystal, *i.e.* to consist of the same type of clusters.

We employed the cluster approach to $cF1124$-Cu$_{56.9}$Cd$_{43.1}$ similar to the structures discussed above (see Fig. 9). The cluster shells found around the points of highest symmetry ($\bar{4}3m$) are less regular when their centers are formed by more than one atom. The positions $4a$ $0, 0, 0$ and $4d$ $\frac{3}{4}, \frac{3}{4}, \frac{3}{4}$ are surrounded by octahedra, which are not considered to be full cluster shells but rather a somewhat large cluster center; in this case not even the first cluster shell exhibits any considerable regularity. Around $4b$ $\frac{1}{2}, \frac{1}{2}, \frac{1}{2}$, where a small tetrahedron is centered that cannot be regarded as an independent cluster shell either, a quite low cluster symmetry is also observed:
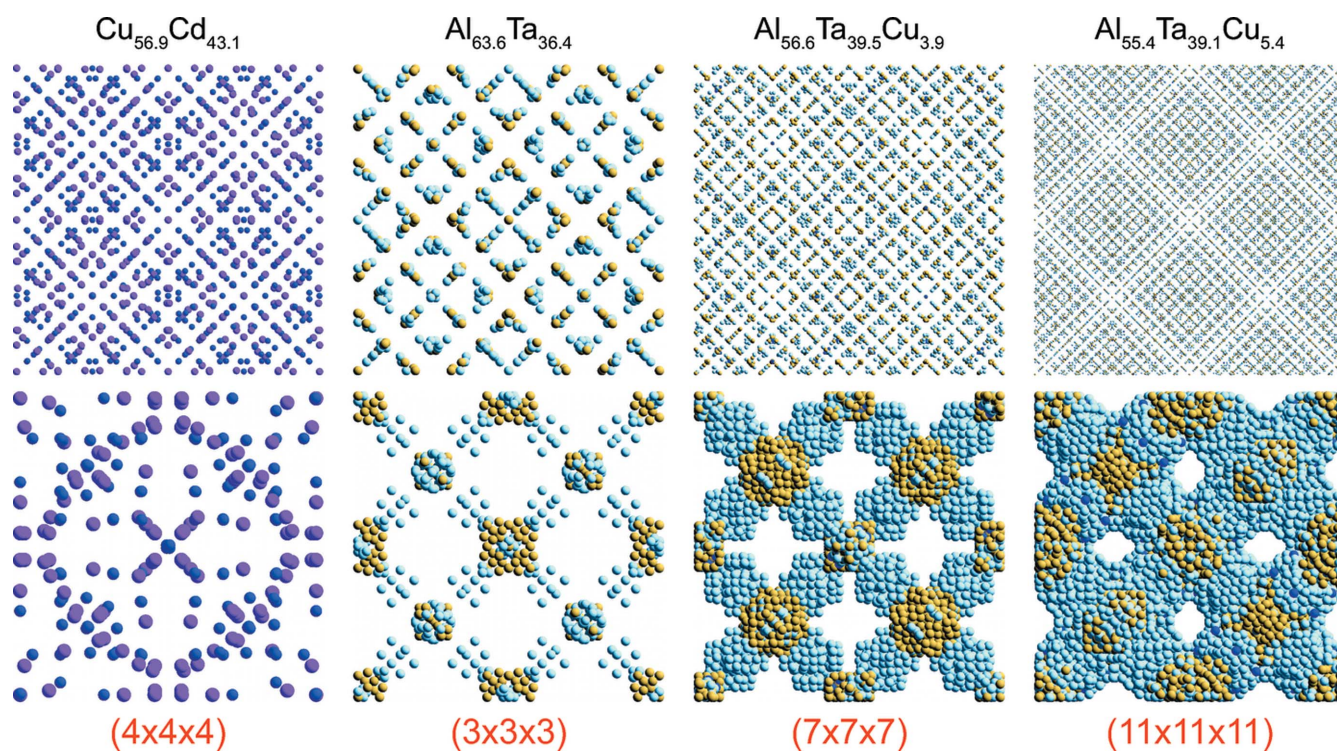

Cu$_{56.9}$Cd$_{43.1}$ Al$_{63.6}$Ta$_{36.4}$ Al$_{56.6}$Ta$_{39.5}$Cu$_{3.9}$ Al$_{55.4}$Ta$_{39.1}$Cu$_{5.4}$

(4x4x4)   (3x3x3)   (7x7x7)   (11x11x11)

Figure 8
Unit cells of the bigger complex intermetallic structures in the space group $F\bar{4}3m$ (superstructures with $p = 4, 7, 11$), as well as Al$_{63.6}$Ta$_{36.4}$ for comparison with the Al–Ta–Cu structures. Shown are the projection of the unit cell along the [001] direction (upper) and a similar projection of the respective average structure (lower).

already the first shell is a rather irregular 22-atom polyhedron with tetrahedral symmetry and only triangular faces. The second shell is a F_{40}^{22} fullerene-like polyhedron with only
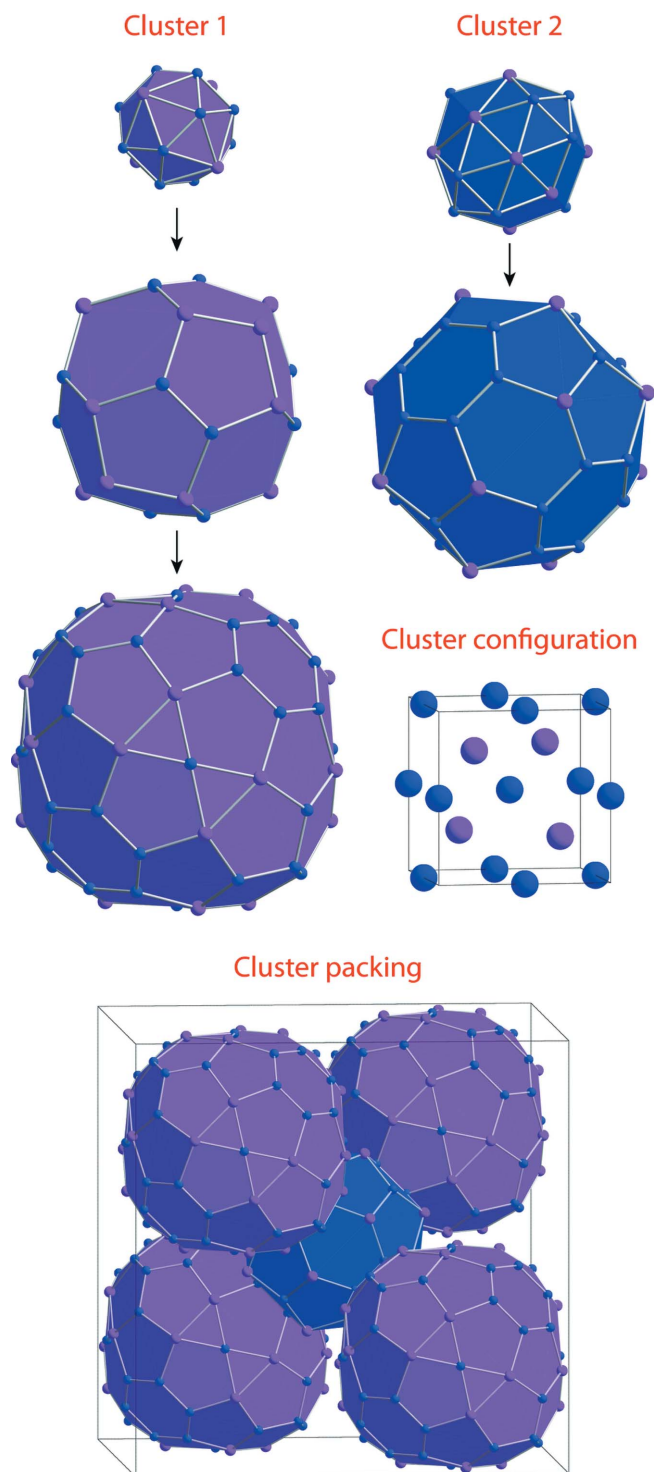

Cluster 1

Cluster 2

Cluster configuration

Cluster packing

Figure 9
Cluster structure of the complex intermetallic compound $Cu_{56.9}Cd_{43.1}$ in the space group $F\bar{4}3m$. Shown are clusters 1 and 2 up to shells three and two, as well as the cluster structure built from them. Not shown are the atoms capping the p and h faces of the second cluster shell in cluster 1. The cluster configuration is the same as for the $cF \simeq 400$ structures, with additional intermediate clusters at $\frac{1}{2}\frac{1}{2}\frac{1}{2}$ and corresponding positions.

partially capped p and h faces. The cluster shells around $4c$ $\frac{1}{4},\frac{1}{4},\frac{1}{4}$, occupied by a Cd atom, are the most regular ones: first – a Friauf polyhedron FK_{16}^{28}; second – a F_{28}^{16} fullerene-like cluster with all 12 p faces capped by one atom each and the four h faces by three atoms each, thus producing a 52-atom cluster shell; third – a 70-atom polyhedron consisting of 12 triangles, 36 pentagons and four hexagons, capped yielding a 110-atom polyhedron FK_{110}^{266}. The 70-atom polyhedra around $4c$ and F_{40}^{22} around $4b$ share hexagonal faces and build an infinite three-dimensional network. This packing and the cluster shells involved are shown in Fig. 9. The rest of the structure is explained by the icosahedral network as discussed in the previous work on this compound (Samson, 1967; Kreiner & Schäpers, 1997).

3.4. (110) layers

As already mentioned above, the (110) layers play a major role in structures with symmetry $F\bar{4}3m$. They contain atomic positions belonging to all special Wyckoff sites and therefore are representative of the structure as a whole. The (110) layers of the five structure variants with space-group symmetry $F\bar{4}3m$ and $Fd\bar{3}m$ are shown in Fig. 10.

If the framework of symmetry elements in space group $F\bar{4}3m$ is considered, it is obvious that the atomic arrangement on the (110) plane is not only repeated with translations [110] or $[\frac{1}{2}\frac{1}{2}0]$ but also $[\frac{1}{4}\frac{1}{4}0]$ and $[\frac{3}{4}\frac{3}{4}0]$. These layers coincide with mirror planes and therefore are flat. Halfway between two mirror planes, a glide plane is located. On both sides of it, puckered atomic layers can be found in the investigated structures. As a result, the whole unit cell can be described by flat (f) and puckered layers (p), stacked $f, p, -p', f', p', -p, f$.[8]

Thus, between two symmetrically related flat layers two puckered ones are found for the $(3 \times 3 \times 3)$-fold superstructures. In the case of higher-order superstructures with $p = 7$ and $p = 11$, six and ten layers are sandwiched between two flat ones. This corresponds to three and five symmetrically independent puckered layers on one side of the glide plane. This means that two, four and six symmetrically independent layers are needed to describe the $(p = 3, 7, 11)$ structures along a [110] direction; one of these is always a flat layer. The layer-stacking period thus corresponds directly to the order of the superstructure.

4. Structures with space-group symmetry $Fd\bar{3}m$

Among the nine intermetallic compounds on our list with space group symmetry $Fd\bar{3}m$, two have significantly larger unit cells than the others: the famous Samson phase $cF(1192 - 23)$-$Al_{53.6}Mg_{46.4}$ and the closely related structure $cF(1192 - 40)$-$Cd_{66.7}Na_{33.3}$, also found by Samson (1962, 1965). The remaining seven compounds are $(3 \times 3 \times 3)$-fold superstructures of what seems to be a similar basic structure to the previously discussed compounds in space group $F\bar{4}3m$, which is a subgroup of index 2 of $Fd\bar{3}m$.

---

[8] Here p and $-p$ lie on opposing sides of a mirror plane and p' is generated from p after a glide operation.
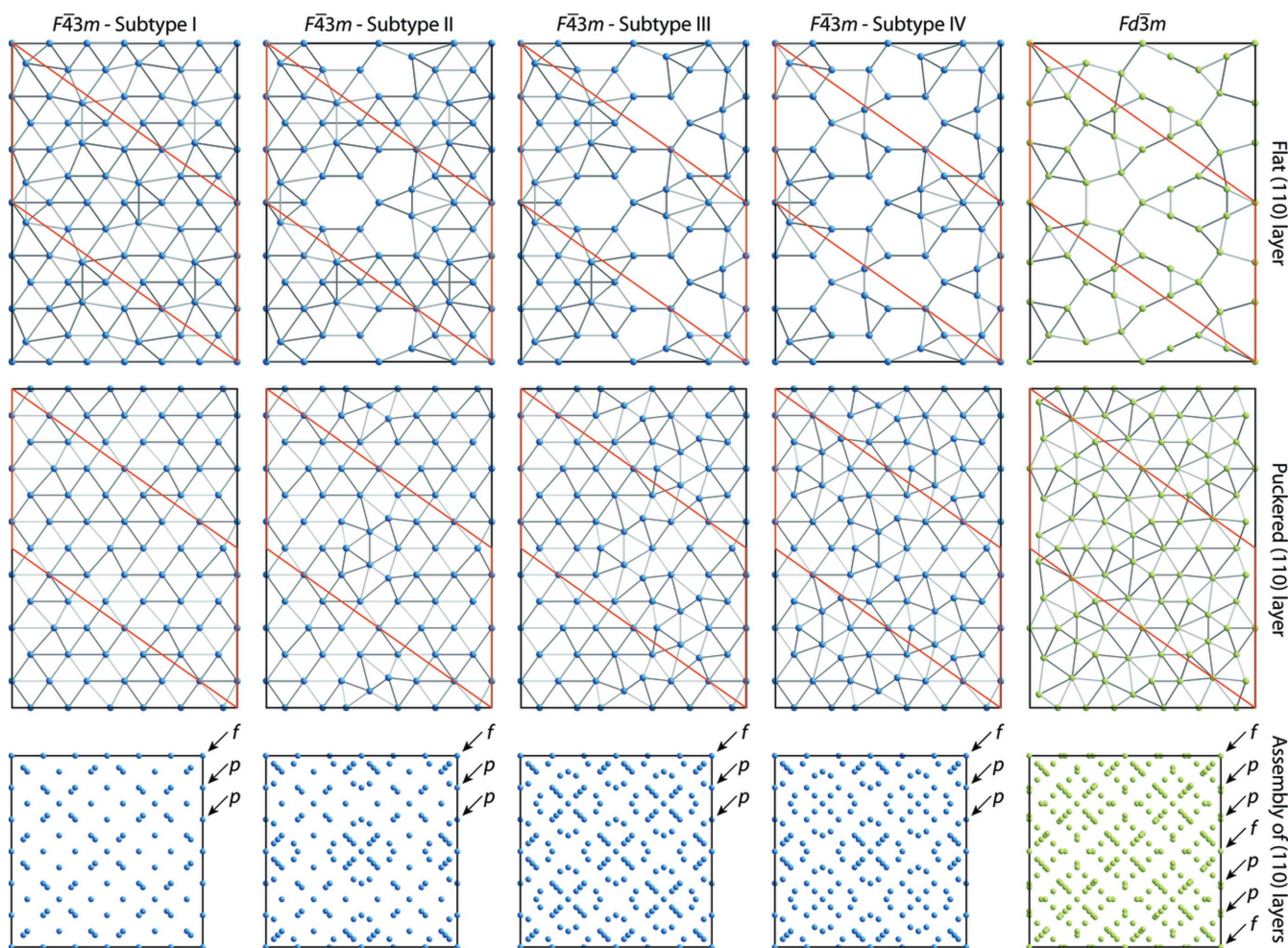
Figure 10
(110) layers of cubic complex intermetallics in the $F\bar{4}3m$ and $Fd\bar{3}m$ space groups. Both the flat as well as the puckered layers can be derived from hexagonal dense packed arrangements containing differing amounts of defects. Shown on the right side are projections of the unit cells along [100], where the layer arrangement can be seen.

4.1. (3 × 3 × 3)-fold superstructures – cF464

The six p^3-fold superstructures ($p = 3$) in space group $Fd\bar{3}m$ are listed in Table 1; their lattice parameters ($19.8 < a < 24.3$ Å) are in the same range as those of the lower-symmetric compounds. The atomic sites featured in those structures are strikingly similar (Table 3). Only cF472-$Zn_{61.0}Ca_{35.6}Ni_{3.4}$ shows minor deviations: Ni atoms are located at the Wyckoff position 16d rather than 8a. The unit cell and average structure of one representative of this structure type is shown in Fig. 11.

The Wyckoff positions in space group $Fd\bar{3}m$ obviously have double multiplicity with respect to the space group $F\bar{4}3m$ owing to the symmetrically equivalent positions created by the inversion center added at $\frac{1}{8}, \frac{1}{8}, \frac{1}{8}$. To compare structures in both symmetries, origin choice 1 has been used in the case of space group $Fd\bar{3}m$, as it directly corresponds to the setting of $F\bar{4}3m$.

Looking for a cluster structure similar to that introduced for cF444-$Al_{63.6}Ta_{36.4}$ (Conrad *et al.*, 2009), one finds a quite regular three-shell cluster centered at Wyckoff position 8a

(see Fig. 12). Its innermost shell is a Friauf polyhedron, followed by a capped fullerene-like polyhedron F_{28}^{16}, a truncated triakistetrahedron which is the dual of a Friauf polyhedron.

The third cluster shell, a fullerene of type F_{84}^{44}, is again the dual of the capped F_{28}^{16} polyhedron. These outer cluster shells already interpenetrate each other, while the second shells share all their hexagonal faces (see Fig. 12), which results in a tetrahedral coordination of every F_{28}^{16} with four polyhedra of the same type. This network is completed with a second type of cluster, centered at the generally empty sites of Wyckoff position 16d $\frac{5}{8}, \frac{5}{8}, \frac{5}{8}$, with an icosahedron as the first shell and a pentagonal dodecahedron around it, as shown in Fig. 12. Four of these dodecahedra meet at 8b $\frac{1}{2}, \frac{1}{2}, \frac{1}{2}$ and, together with the F_{28}^{16} polyhedra, completely fill space.

The sites of this structure type with space group $Fd\bar{3}m$ can largely be related directly to sites of the corresponding structures in $F\bar{4}3m$. Therefore, their cluster descriptions should be similar. The corresponding inner cluster shells are easily recognizable: only the Friauf polyhedra have to be

Table 3
Atomic sites of the here-discussed cubic complex intermetallics in space group $Fd\bar{3}m$.

Not included are the coordinates of the slightly deviating $Zn_{61.0}Ca_{35.6}Ni_{3.4}$ structure. The Wyckoff site is included in the site label. The idealized positions, used for graphics of polyhedra, are also given.

Site	Symmetry	$\bar{x}(3\sigma)$	$\bar{y}(3\sigma)$	$\bar{z}(3\sigma)$	Idealized coordinates
8a	$\bar{4}3m$	0.25	0.25	0.25	1/4 1/4 1/4
8b	$\bar{4}3m$	0.5	0.5	0.5	1/2 1/2 1/2
32e1	$.3m$	0.165 (8)	x	x	1/6 1/6 1/6
32e2	$.3m$	0.405 (8)	x	x	39/96 39/96 39/96
96g1	$..m$	0.439 (6)	x	0.251 (14)	21/48 21/48 1/4
96g2	$..m$	0.204 (5)	x	0.391 (13)	5/24 5/24 9/24
96g3	$..m$	0.164 (5)	x	0.509 (14)	1/6 1/6 1/2
96g4	$..m$	0.207 (3)	x	0.617 (8)	5/24 5/24 15/24

taken into account, not the alternative rhombic dodecahedra in subtypes I–IV. The second shell can be directly related by atomic sites: *e.g.* around 4c, sites 16e2 and 48h1–48h3 constitute the FK_{40}^{76} cluster and only 48h3 has to be omitted to obtain a distorted version of F_{28}^{16}.

The sites forming the different clusters as well as their correspondence to the sites in space group $F\bar{4}3m$ are given in Tables 22 and 23 of the supplementary material.

4.2. (4 × 4 × 4)-fold superstructures – cF1192

The first structure of this unit cell size to be reported was $cF(1192 - 40)$-$Cd_{66.7}Na_{33.3}$ (Samson, 1962). It was found to be built up of Friauf polyhedra, arranged in five-rings, as usually described by their *tt* skeleton. Six of these five-rings are again

arranged centered at the vertices of a tetrahedrally distorted octahedron and produce four more Friauf polyhedra at the vertices of a tetrahedron around their common center. The whole structure is made up by this arrangement, complemented by even more Friauf polyhedra between them as well as 32 additional atoms. For the structure solution of this highly complex structure, so-called packing maps were employed (Samson, 1964). Later, similar coordinates resulting in an improved structure model could be calculated from coincidence site lattice theory (Yang *et al.*, 1987). The purely geometrical understanding of the structure was recently complemented by quantum-mechanical calculations (Lee *et al.*, 2007; Fredrickson *et al.*, 2007), indicating that the structure can be divided into electron-rich and -poor substructures.

The more famous 'Samson phase' $cF(1192 - 23)$-$Al_{53.6}Mg_{46.4}$ (Samson, 1965) can be regarded as isostructural with $cF(1192 - 40)$-$Cd_{66.7}Na_{33.3}$ and is also nearly exclusively built from Friauf polyhedra, although it exhibits a considerable degree of disorder. Samson attributed this to the formation of a large number of icosahedra in the structure, which finally outnumber the Friauf polyhedra by far. An extensive re-investigation and further analysis of $Al_{53.6}Mg_{46.4}$ with respect to structure and related properties was recently carried out and confirmed the previous structure model in detail (Feuerbacher *et al.*, 2007). A description of the structure by layers was done by Wolny *et al.* (2008), where also the interplay between these layers and previously described clusters is discussed (Sikora *et al.*, 2008).

The two isostructural compounds can be described in a similar way to the smaller structures by the cluster approach (see Fig. 13). Projections of the unit cells, as well as of their average structures are shown in the overview in Fig. 11. The clusters centered at 8a 0,0,0 (around a small tetrahedron that cannot be regarded as an independent cluster shell) do not exhibit a high degree of symmetry: the first shell is a rather irregular 22-atom cluster with tetrahedral symmetry and only triangular faces. The second shell is an incompletely capped fullerene-like F_{40}^{22} polyhedron; this cluster is similar to that found in $cF1124$-$Cu_{56.9}Cd_{43.1}$ centered at site 4b (see Fig. 9).

The cluster centered around 8b $\frac{1}{2},\frac{1}{2},\frac{1}{2}$ (where atoms are located in both mentioned compounds), on the other hand, is fairly regular and has the following cluster shells: first – a Friauf polyhedron FK_{16}^{28}; second – a F_{28}^{16} fullerene-like cluster with all faces capped yielding a FK_{44}^{84} polyhedron; third

$In_{70.7}K_{29.3}$ $Cd_{66.7}Na_{33.3}$ $Al_{53.6}Mg_{46.4}$
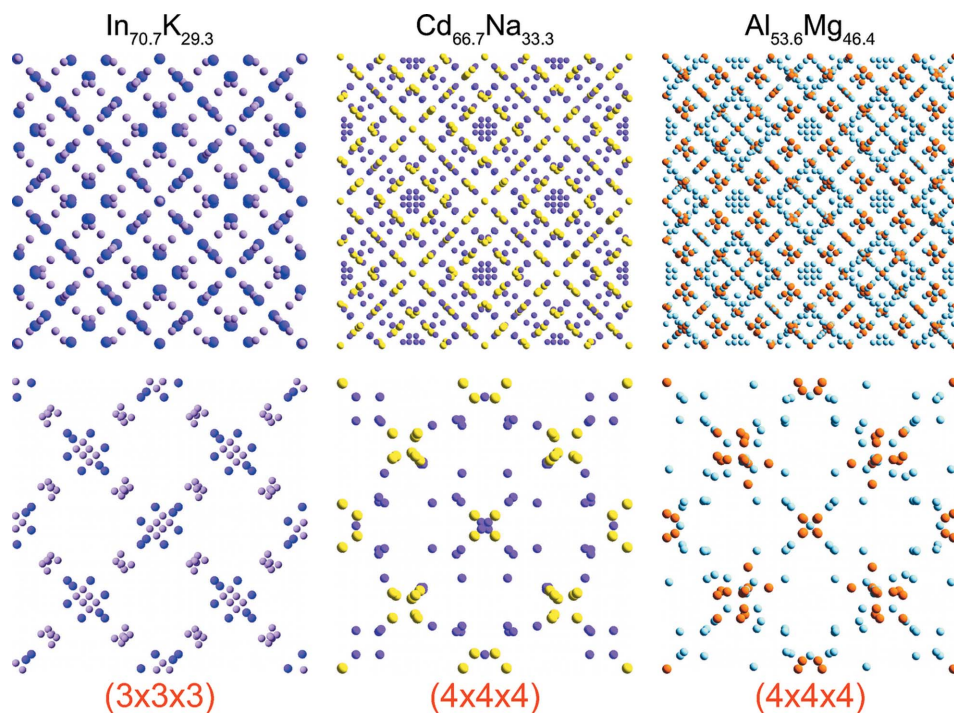
(3x3x3) (4x4x4) (4x4x4)

Figure 11
Unit cells of the complex intermetallic structures in the space group $Fd\bar{3}m$. Shown are the projection of the unit cell along the [001] direction (upper) and a similar projection of the respective average structure (lower).

– a F_{76}^{40} cluster with all faces capped resulting in a FK_{116}^{228} polyhedron (fourth – a 114-atom shell consisting of 76 triangles, 12 pentagons and 28 hexagons). The second cluster shells
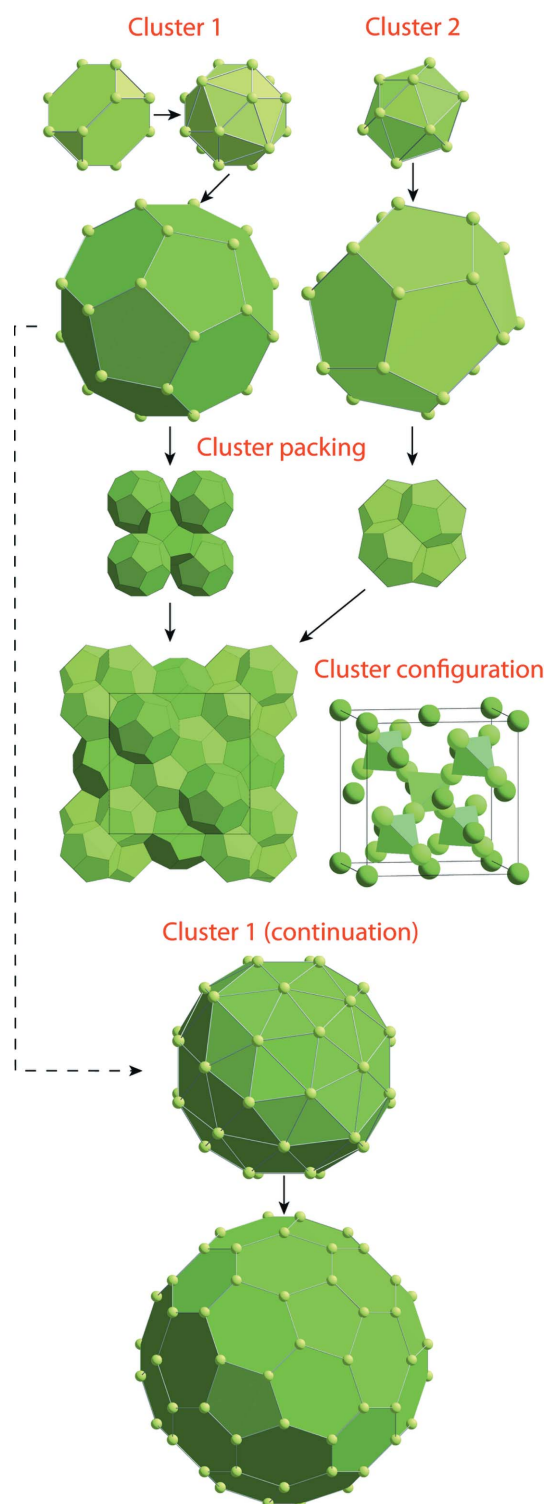
around 8*b* do not touch each other, but the third cluster shells overlap. The F_{76}^{40} polyhedron and the two-shell clusters around 8*a* together describe all atomic positions of the discussed structures. Hereby the F_{76}^{40} clusters, which are identical to those found in subtypes III and IV of the *cF*464 structures in $F\bar{4}3m$, are arranged on a diamond-like lattice and overlap with their
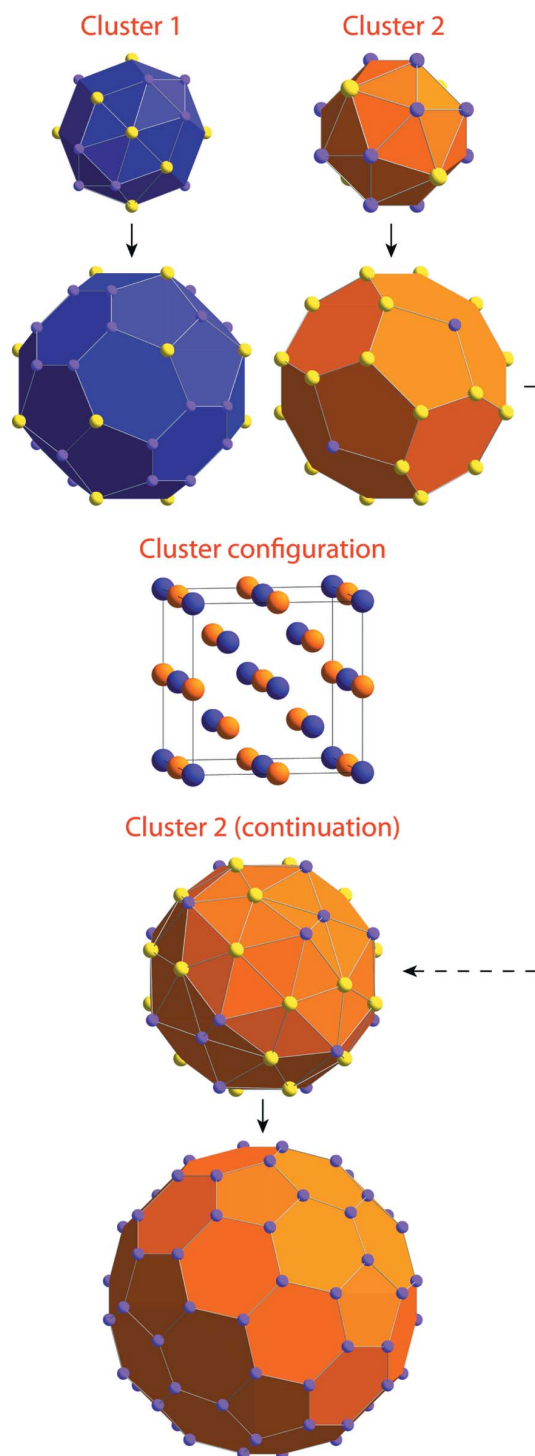

Figure 12
Cluster structure of complex intermetallics *cF*464 in space group $Fd\bar{3}m$. Shown are clusters 1 and 2 up to shells three and two, as well as the cluster structure, built solely of two-shell clusters. The cluster configuration shown corresponds to this two-shell variant, whereas the three-shell clusters pack similarly to those in $F\bar{4}3m$, when symmetry is reduced (otherwise they interpenetrate).

Figure 13
Cluster structure of complex intermetallics *cF*1124 in space group $Fd\bar{3}m$. Shown are clusters 1 and 2 up to shells two and three, respectively, as well as the cluster configuration in the unit cell.

third shells. The configuration of cluster centers as well as the clusters' first two (8a) or three (8b) shells are shown in Fig. 13.

5. Structures with other space-group symmetries

Besides the 48 structures on our list with symmetries $F\bar{4}3m$ and $Fd\bar{3}m$, only eight more are known with other cubic symmetries; their projections are shown in Fig. 14.

5.1. Four structures in $Fm\bar{3}m$ – ($4 \times 4 \times 4$)-fold super-structures

The structure of $cF(1208 - 64)$-$Dy_{40.9}Sn_{39.2}Co_{19.9}$ was determined in space group $Fm\bar{3}m$ without any in-depth discussion of its building units (Salamakha *et al.*, 2001). It is closely related to $cF1124$-$Tb_{41.6}Ge_{39.9}Fe_{18.5}$ (Pecharskii *et al.*, 1987) as well as the corresponding structures in the Pr–Sn–Co and Gd–Ge–Fe systems. Here we discuss a possible cluster description of the structure (see Fig. 15).

Around $4a$ $0, 0, 0$, occupied by a Dy atom, the following cluster shells are found: first, a disordered rhombic dodeca-hedron/capped cuboctahedron (in $Tb_{41.6}Ge_{39.9}Fe_{18.5}$, only the latter is present); second, a capped rhombicuboctahedron/deltoidal icositetrahedron; third, an 80-atom polyhedron with six quadrangular and 144 triangular faces. Around $4b$ $\frac{1}{2}, \frac{1}{2}, \frac{1}{2}$, occupied by a Co atom, the cluster shells are as follows: first, a cube; second, a capped rhombicuboctahedron/deltoidal icosi-tetrahedron; third, a 48-atom polyhedron with eight triangular and 42 quadrangular faces.

The sites of Wyckoff position $8c$ $\frac{1}{4}, \frac{1}{4}, \frac{1}{4}$ and $\frac{3}{4}, \frac{3}{4}, \frac{3}{4}$ are each occupied by an atom, surrounded by a 22-atom cluster shell with triangular faces, just as found in the $F\bar{4}3m$ and $Fd\bar{3}m$ compounds of similar unit-cell size at positions $4b$ and $8a$. The second shell is the same 28-atom cluster as was previously found in the $cF(464 - x)$ compounds: a tetrahedrally trun-cated rhombic dodecahedron, with capping atoms resulting in a FK_{40}^{76} polyhedron.

The two three-shell clusters at positions $4a$ (cluster 1) and $4b$ (cluster 2) and the four-shell cluster at $8c$ (cluster 3) pack densely describing these two structures entirely. The first two clusters share quadrangular faces along all $\langle 100 \rangle$ directions and are aligned alternately in those directions. The cubic interstices in this structure are filled with $8c$ polyhedra, which share one triangular face with each neighboring three-shell cluster at $4b$ and six triangular faces with each cluster at $4a$. The clusters and their arrangement are shown in Fig. 15.

5.2. Three structures in $Fm\bar{3}c$

The structure of $cF(944 - 22)$-$Zn_{67.1}Sn_{20.8}Mo_{12.1}$ was described in the space group $Fm\bar{3}c$ (Hillebrecht *et al.*, 1997). It looks somewhat unusual with respect to the number of atoms per unit cell compared with the other structures discussed here containing either ~ 400 or ~ 1200 atoms per unit cell. Furthermore, it has a rather ill-defined ($4 \times 4 \times 4$)-fold superstructure.

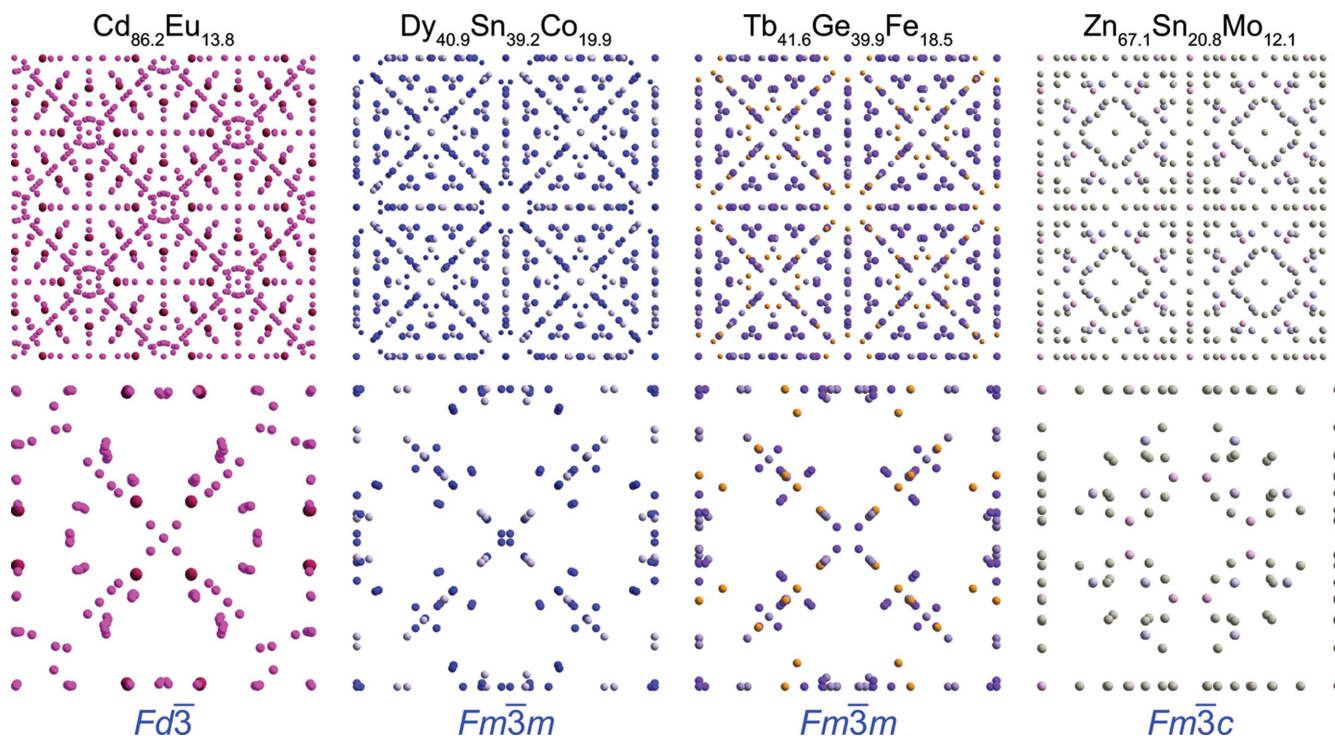| $Cd_{86.2}Eu_{13.8}$	$Dy_{40.9}Sn_{39.2}Co_{19.9}$	$Tb_{41.6}Ge_{39.9}Fe_{18.5}$	$Zn_{67.1}Sn_{20.8}Mo_{12.1}$
$Fd\bar{3}$	$Fm\bar{3}m$	$Fm\bar{3}m$	$Fm\bar{3}c$

Figure 14
Unit cells of the $cF \simeq 1000$ complex intermetallic structures in the remaining space groups $Fd\bar{3}$, $Fm\bar{3}m$ and $Fm\bar{3}c$. Shown are the projections of the unit cells along the [001] direction (upper) and similar projections of the respective average structures (lower).

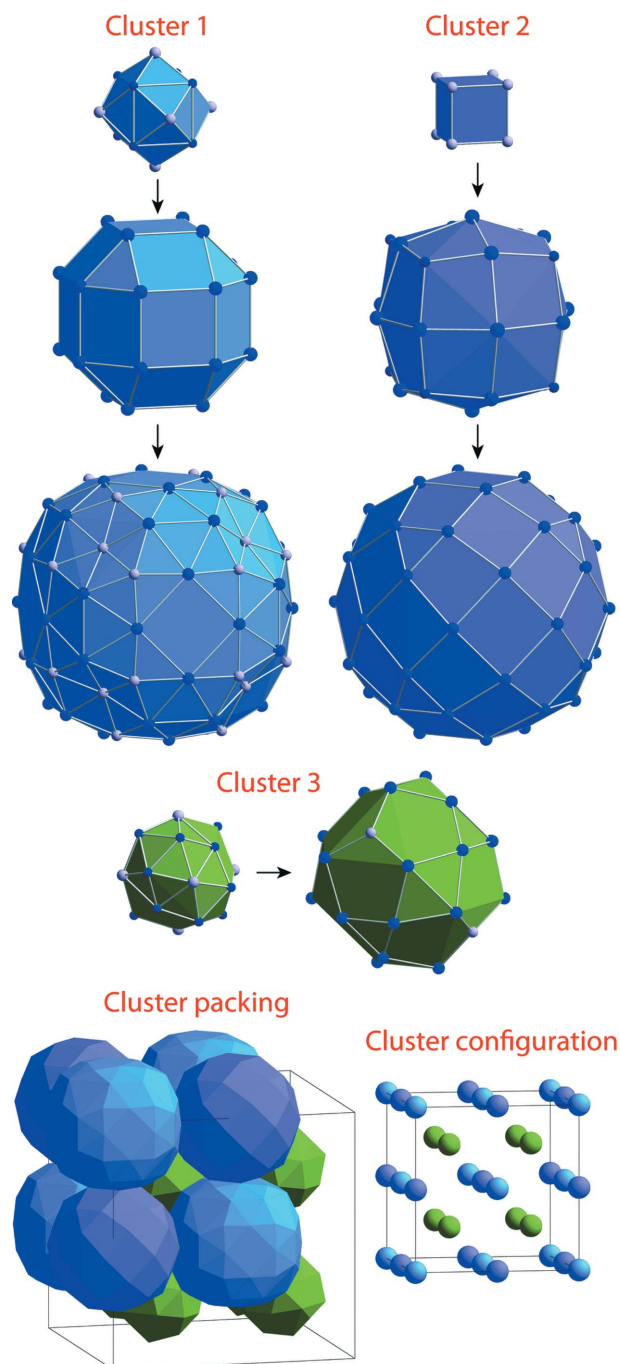**Figure 15**
Cluster structure of complex intermetallics in space group $Fm\bar{3}m$. Shown are clusters 1 and 2 with all three shells and cluster 3 with two shells, as well as the arrangement of these clusters in the structure and the arrangement of cluster centers within the unit cell.

The cluster structure has already been introduced by Hillebrecht *et al.* (1997) and features the following nested clusters around the two highest-symmetric sites (see Fig. 16): at $8a\ \frac{1}{4},\frac{1}{4},\frac{1}{4};\frac{3}{4},\frac{3}{4},\frac{3}{4}$ a centered rhombic dodecahedron within a snub cube[9] with a 60-atom third-shell cluster, consisting of 24

pentagonal, six quadrangular and 24 triangular faces (cluster 1); and around $8b\ 0,0,0$ and $\frac{1}{2},\frac{1}{2},\frac{1}{2}$ a centered icosahedron within an icosidodecahedron with atoms capping all pentagonal faces within a small rhombicosidodecahedron[10] (cluster 2). The symmetrically inequivalent three-shell clusters overlap and cover all sites within the unit cell. If one considers a two-shell cluster on one of the sites $8a$ and $8b$ and a three-shell cluster on the other, they form a packing which describes the structure entirely. The different cluster shells as well as both packing alternatives are shown in Fig. 16.

The structures $cF(968-32)$-$Zn_{57.3}Ru_{22.2}Sb_{20.5}$ and $cF(992-125)$-$Zn_{76.9}Ru_{12.0}Sb_{11.1}$ were found to be nearly isostructural to $cF(944-22)$-$Zn_{67.1}Sn_{20.8}Mo_{12.1}$ (Xiong *et al.*, 2010). They exhibit minor differences, as well as a certain range of compositions in the latter case, leading to a solid solution with exchange of Sb and Zn, as described in detail by Xiong *et al.* (2010).

5.3. One structure in $Fd\bar{3}$ – a $(4 \times 4 \times 4)$-fold superstructure

The structure of $cF1392$-$Cd_{86.2}Eu_{13.8}$, with symmetry $Fd\bar{3}$, is an approximant structure to the binary icosahedral quasi-crystals in the Ca–Cd and Yb–Cd systems (Gómez & Lidin, 2004). It was described by two symmetrically inequivalent triacontahedra with the following inner shells (from inside to outside): tetrahedron, dodecahedron, icosahedron and icosidodecahedron. Additionally, interstitial atoms had to be introduced.

In our cluster description (see Fig. 17), the tetrahedron forms the cluster center and the surrounding dodecahedron the first cluster shell. The next two polyhedra are joined so that the second cluster shell is an icosidodecahedron whose pentagonal faces are capped (by the Eu atoms which – according to the previous description – belong to the icosahedron). The third cluster shell then consists of the atomic sites which were previously discussed as building a triaconta-hedron and belonging to some interstitial cubes. All of those atoms build a fullerene-like shell F_{80}^{42} with icosahedral symmetry. There are two symmetrically inequivalent versions of this three-shell cluster, which overlap with each other as well as with clusters of the symmetrically non-related type. The cluster centers are located at the positions $8a\ 0,0,0$ and $8b\ \frac{1}{2},\frac{1}{2},\frac{1}{2}$, and arranged in a double-diamond lattice. The three-shell clusters around one of these centers already overlap in the outer shell. The clusters, as well as their arrangement in the unit cell, are shown in Fig. 17. The three-shell cluster around $8a$ and the two-shell cluster around $8b$ together describe all the atoms present in the published structure.[11]

---

[9] A snub cube is an Archimedean solid with 32 triangular and six square faces, and 24 vertices.

[10] This polyhedron is often simply called rhombicosidodecahedron (r), but is referred to as 'small r'. Also termed 'truncated r' in order to distinguish it from the 'great r' (Cundy & Rollett, 1961).

[11] The Wyckoff positions in space group $Fd\bar{3}$ correspond directly to those in $Fd\bar{3}m$, with the exception of two of the highest multiplicities ($96h \rightarrow 96g$, $192i \rightarrow 2 \times 96g$).
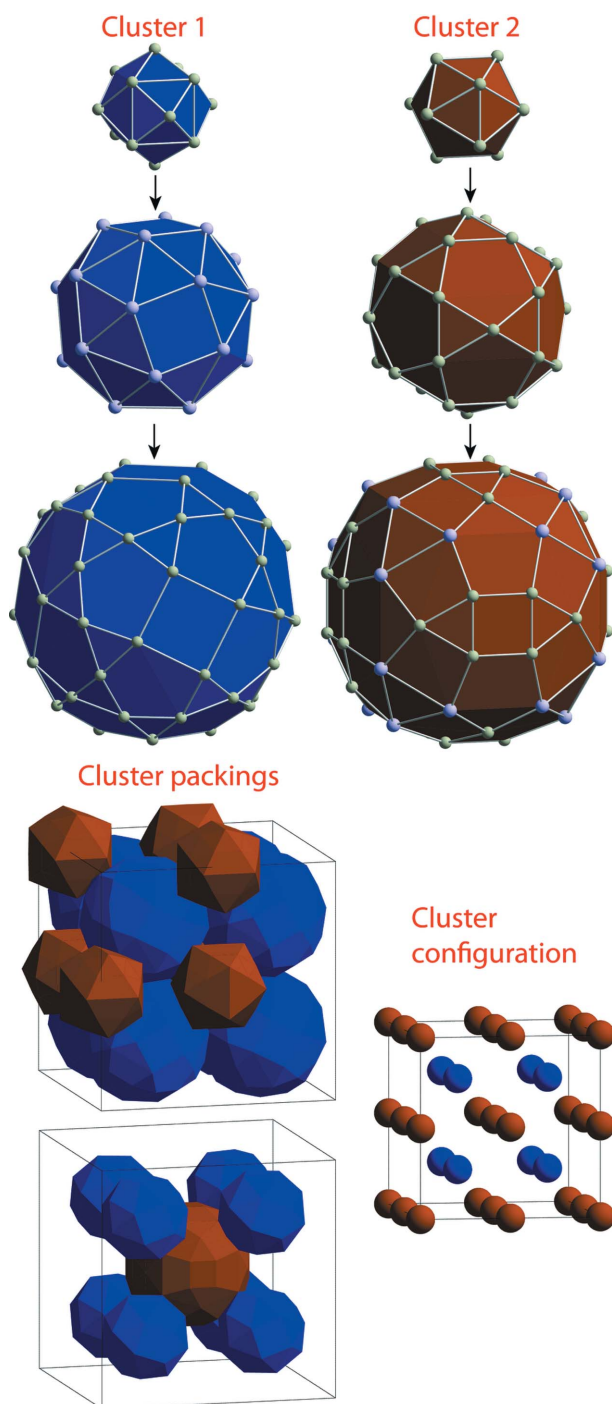
Figure 16
Cluster structure of complex intermetallics in space group $Fm\bar{3}c$. Shown are clusters 1 and 2 with all three shells, as well as the two possible packing arrangements of these clusters in the structure and the arrangement of cluster centers within the unit cell.

6. First-principles studies

The electronic properties of the structures were studied by *ab initio* calculations. With respect to computational feasibility, these were restricted to compounds with less than 500 atoms per f.c.c. unit cell, thus not including the Samson phase and

structures of higher complexity. Prior to calculations, the structures were transformed to their primitive rhombohedral setting using the matrix

$$\begin{pmatrix} 0 & \frac{1}{2} & \frac{1}{2} \\ \frac{1}{2} & 0 & \frac{1}{2} \\ \frac{1}{2} & \frac{1}{2} & 0 \end{pmatrix},$$

resulting in not more than 116 atoms per unit cell with lattice parameters $a_{\mathrm{rhomb}} = a_{\mathrm{cub}}/\sqrt{2}$ and $\alpha = 60°$. All calculations discussed in the following are based on these primitive unit cells.

Due to the already large number of atoms per unit cell we could not increase the number of unit cells in our calculations to treat structural disorder properly. Consequently, our structure models had to be idealized for the calculations. For that purpose partially occupied and split positions were condensed into fully occupied, single ones and occupancies of deficient sites were rounded to full or zero occupancy. Mixed positions were assumed to be fully occupied by the majority element on the respective site. Details on the performed idealization are given in Tables 27 and 28 of the supplementary material.

The structures of $cF(416 - 16)$-$Cu_{73.9}Sn_{23.2}Ni_{2.9}$ and $cF(416 - 1)$-$Zn_{86.6}Fe_{6.7}Ni_{6.7}$ had to be calculated in the variants $Cu_{76.8}Sn_{23.2}$, $Zn_{86.6}Fe_{13.4}$ and $Zn_{86.6}Ni_{13.4}$, because the Ni sites had not been specified explicitly by the authors (Booth *et al.*, 1977; Lidin *et al.*, 1994). Also the structure of $cF464$-$Ga_{53.4}Li_{31.0}Cu_{8.6}In_{6.9}$ was reduced to $Ga_{62.1}Li_{31.0}Cu_{8.6}$, and thus a ternary compound, since In atoms were only found as minority elements on shared sites (Chahine *et al.*, 1995).

The calculations were performed with the *VASP* (Vienna *ab initio* simulation package) code (Kresse & Furthmüller, 1996a,b). The generalized gradient approximation (GGA; Perdew *et al.*, 1996) together with the projector-augmented wave (Blöchl, 1994) method have been applied to optimize the structures and calculate the charge distribution (at 0 K). In all calculations the projector-augmented wave (PAW) potentials and a $4 \times 4 \times 4$ Monkhorst–Pack scheme (Monkhorst & Pack, 1976) for the Brillouin zone sampling, as provided by the code, were employed. The positions of all atoms were relaxed with the conjugate gradient method. For the cut-off of the plane wave representation of the wavefunction, the default values were used. The energy minimization procedure is iterative and proceeds until self-consistency within a prescribed tolerance of 10^{-4} eV per unit cell for electronic optimization and 10^{-3} eV per unit cell for atomic relaxation.

6.1. Electron localization function

The electron localization function (*ELF*; Becke & Edgecombe, 1990; Silvi & Savin, 1994) is a measure of the likelihood of finding an electron in the neighborhood space of a reference electron located at a given point and with the same spin. Physically this measures the extent of spatial localization of the reference electron and provides a method for the mapping of electron pair probability in multi-electronic systems. The *ELF* represents the organization of chemical

bonding in direct space. It is a dimensionless localization index that expresses electron localization with respect to the uniform electron gas, whereas $ELF = 1$ corresponds to perfect localization and $ELF = 0.5$ to the electron gas. In most metals there would not be any ELF maxima between the atoms but only around their centers, reflecting the shell structure of the core electrons. The ELF was calculated with the corresponding module provided with the $VASP$ code. For an overview, see the ELF website (http://www.cpfs.mpg.de/ELF).

Even though the underlying structural building principles are the same, the ELF maps are quite diverse. Structures with the same chemical environment locally will of course exhibit the same ELF map behavior, but the overall ELF map can change significantly simply with a change of composition, $e.g.$ the Zn–Pt system in subtype I of the $F\bar{4}3m$ structures, depicted in Fig. 4 of the supplementary material. On the other hand, structures with almost the same electronic composition such as Mg-(Ir,Pd,Rh,Ru) exhibit almost identical ELF maps, depicted in Fig. 3 of the supplementary material.

In our case the calculated ELF maps can be roughly divided into two groups: one with significant electron localization and another without. Structures of the second category include nearly all compounds with majority elements Zn and Cu as well as $cF432$-$Li_{64.3}In_{26.5}Ag_{9.2}$. Representative ELF maps of the first group of structures are shown in Fig. 18 and discussed in the following. The ELF maps of all discussed structures are given in Figs. 3, 4, and 5 of the supplementary material.

In the following the most distinct features in the different ELF maps are given:

(i) triangular maximum at $16e\ x, x, x$ with $x \simeq 0.365$: $cF420$-$Li_{81.0}M_{19.0}$ (M = Pb, Sn, Ge) (subtype I);

(ii) pentagonal/hexagonal maximum at $24f\ \frac{1}{3}, 0, 0$: $cF408$-$Na_{86.3}Tl_{13.7}$, $cF408$-$Sc_{86.3}Os_{13.7}$, $cF408$-$Mg_{87.3}Ru_{12.7}$, $cF408$-$Mg_{86.3}Rh_{13.7}$, $cF396$-$Mg_{86.3}Ir_{13.7}$/$cF396$-$Mg_{87.9}Ir_{12.1}$, $cF396$-$Mg_{85.9}Pd_{14.1}$ (subtype II);

(iii) dodecahedron around $16e3$:[12] $cF408$-$Mg_{87.3}Ru_{12.7}$, $cF408$-$Mg_{86.3}Rh_{13.7}$, $cF396$-$Mg_{86.3}Ir_{13.7}$, $cF396$-$Mg_{87.9}Ir_{12.1}$, $cF396$-$Mg_{85.9}Pd_{14.1}$;

(iv) shell-like structures around certain sites (especially $16e3$ and $16e4$): $Al_{65.3}Cu_{18.1}Cr_{16.6}$;

(v) covalent bonding between Sc atoms: $cF408$-$Sc_{86.3}Os_{13.7}$.[13]

Generally, the ELF maps are clearly different and show common features only to a very limited extent.

6.2. Bader charge analysis

The Bader analysis (Bader, 1990; Henkelman $et\ al.$, 2006) is an intuitive way of dividing molecules into atoms. The definition of an atom is based purely on the electronic charge density, with zero-flux surfaces being used to divide atoms. A zero-flux surface is a two-dimensional surface on which the

charge density is a minimum perpendicular to the surface. Typically in molecular systems the charge density reaches a minimum between atoms and this is a natural place to separate atoms from each other.

The Bader analysis is used to calculate the volume that a single atom is going to occupy in the structure; additionally the charge within this volume can be integrated, leading to the effective Bader charge on the atom. This allows an estimation of how covalent/ionic/metallic the atom is going to be in the structure. Alternatively, localized charges, not positioned on atoms, can be analyzed, to further investigate the nature of bonding in the structures.

This Bader charge analysis corresponds very well with the ELF maps of the previous section, giving numbers to the
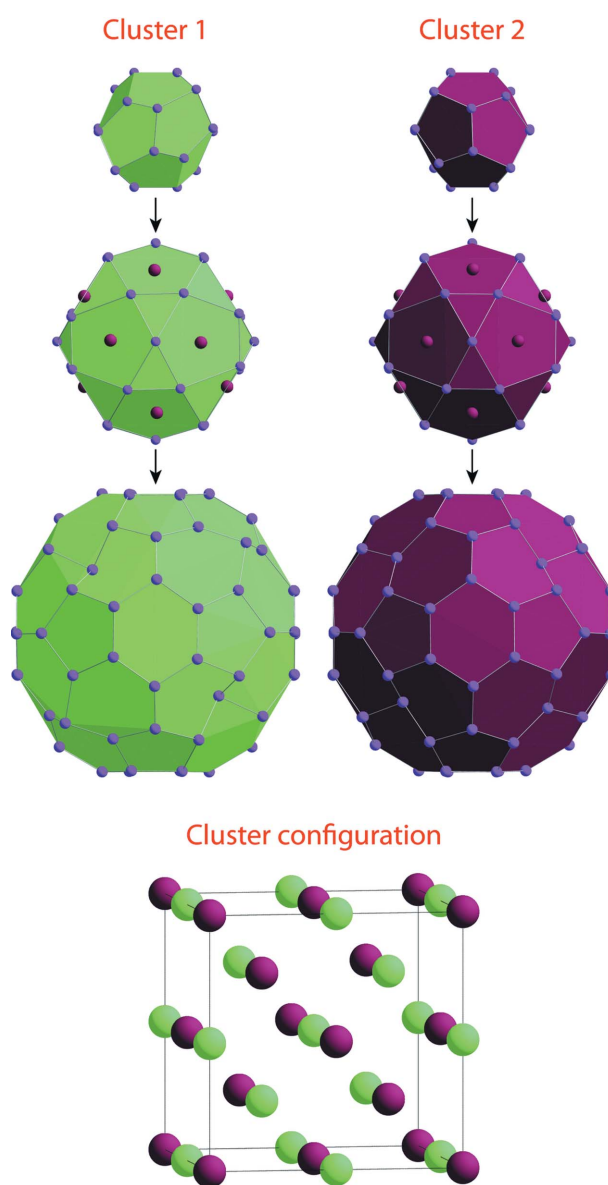

Figure 17
Cluster structure of a complex intermetallic in space group $Fd\bar{3}$. Shown are clusters 1 and 2 up to shell three, as well as the cluster configuration in the unit cell.

---

[12] This feature was also observed in $Zn_{95.3}Mo_{4.7}$ at the same position, but below the threshold for significant ELF values of 0.5.
[13] These ELF maxima connect pairs of Sc atoms with interatomic distances of 4.0–4.6 Å. The shortest Sc—Sc distances in this structure, however, range from 3.0 to 3.9 Å.
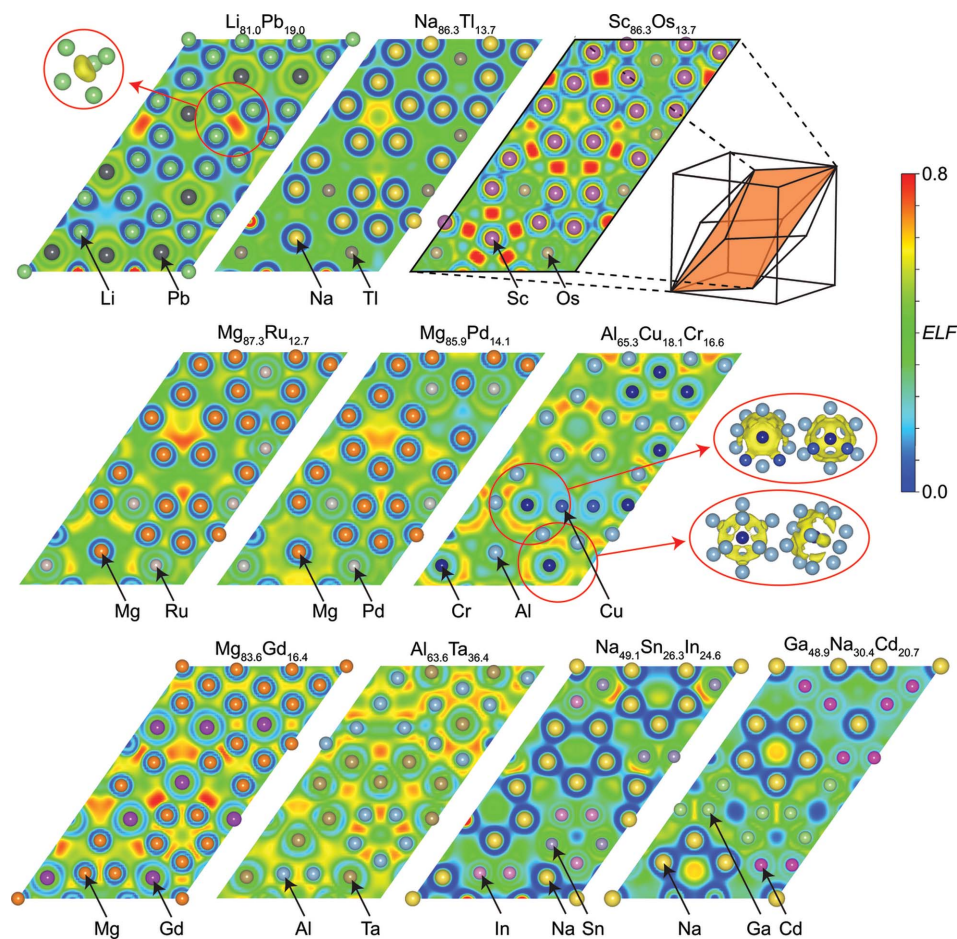
Figure 18
Cuts through the *ELF*s of the following structures: $Li_{81.0}Pb_{19.0}$ ($F\bar{4}3m$, subtype I), $Na_{86.3}Tl_{13.7}$, $Sc_{86.3}Os_{13.7}$, $Mg_{87.3}Ru_{12.7}$, $Mg_{85.9}Pd_{14.1}$, $Al_{65.3}Cu_{18.1}Cr_{16.6}$ (all $F\bar{4}3m$, subtype II), $Mg_{83.6}Gd_{16.4}$, $Al_{63.6}Ta_{36.4}$ (both $F\bar{4}3m$, subtype III), $Na_{49.1}Sn_{26.3}In_{24.6}$ ($F\bar{4}3m$, subtype IV), $Ga_{48.9}Na_{30.4}Cd_{20.7}$ ($Fd\bar{3}m$). Shown are the representative (110) layers of the $F\bar{4}3m$ and $Fd\bar{3}m$ space groups, as they appear in the primitive rhombohedral setting. The insets show the *ELF* three-dimensionally at special sites, visualized with an isosurface level of 0.65 (see legend).

visual interpretation of the maps. No general trends over all structures can be observed. However, within the subtypes and within similar electronic compositions the Bader charges are comparable.

The calculated electron-density distributions were evaluated by means of Bader charge analysis. An overview of the results is given in Table 4. Detailed results are listed in Tables 29 and 30 of the supplementary material.

Some particular features are found in the following compounds:

(i) $cF420$-$Li_{81.0}M_{19.0}$ (M = Pb, Sn, Ge) (subtype I): the considerably heavier M atoms attract the lithium electrons, which lead to an excess of three to four electrons. Additionally, a triangular bond basin was found to be located at the position inside a trigonal Li bipyramid where the *ELF* also exhibited the most distinct maximum. This is pointing to a multi-center bonding behavior of Li in the bipyramid, reflected as well in the Bader charges where the tips of the pyramids are slightly less charged.

(ii) $cF408$-$Na_{86.3}Tl_{13.7}$, $cF408$-$Sc_{86.3}Os_{13.7}$, $Mg_{85-88}TM_{12-15}$ (TM = Ru, Rh, Ir, Pd) (subtype II): the minority atoms are related to a significant electron excess, from -2 to -7, while the majority atoms are found to exhibit slight electron deficiencies. The $Mg_{85-88}TM_{12-15}$ compounds additionally exhibit bond basins with p or h shapes, corresponding to slight deviations in their crystal structure (see section on *ELF*), which hold charges corresponding to 0.4–1.3 electrons.

(iii) $cF408$-$Sc_{86.3}Os_{13.7}$ (subtype II): 41 bilateral bond basins with charges of around 0.3–0.4 electrons correspond to covalent bonding between two atoms at a time, forming a three-dimensional framework of Sc multi-center bonds.[14]

(iv) $cF(448-4)$-$Mg_{83.6}Gd_{16.4}$, $cF444$-$Al_{63.6}Ta_{36.4}$, $cF(448-8)$-$Mg_{82.4}Y_{9.0}Ce_{8.6}$, $cF472$-$Na_{49.2}Ba_{28.8}Li_{22.0}$ (subtype III): the structures also show several bilateral bond basins, which contain integrated charges of 0.1–0.8 electrons. $cF472$-$Na_{49.2}Ba_{28.8}Li_{22.0}$ additionally exhibits one basin in the center of an Li tetrahedron (surrounded by even more Li atoms) with an integrated charge of approximately 4 electrons.

(v) $cF456$-$Na_{49.1}Sn_{26.3}In_{24.6}$ (subtype IV): the Na sites are electron-deficient while the In sites have a slight excess and the Sn a higher excess of electrons. For the Sn with an increase of Na in the local environment, lone electron pairs on the Sn can be observed, resulting in an increase of 0.4 in charge, reflecting the electron transfer from the Na sites.

In summary, a few distinct characteristics can be identified in some of the investigated structures, but they are not consistent throughout one subtype. No overall commonalities can be found for these very similar compounds.

6.3. Electronic density of states

Almost all quasicrystals with icosahedral symmetry have been considered as Hume–Rothery electron compounds, and it has been shown theoretically that the existence of a pseudogap contributes to the stabilization of quasicrystals (Smith & Ashcroft, 1987). This also holds true for phases related to

---

[14] The bond basins found by Bader analysis do not, however, cover all maxima assigned to covalent bond parts from the *ELF*.

Table 4
Bader charges of complex cubic intermetallics $cF464$, ($3 \times 3 \times 3$)-fold superstructures of a common basic structure.

The Bader charges with respect to neutral atoms for the different atomic sorts for all calculated structures are shown. The structures in space group $F\bar{4}3m$ are tagged with their respective subtype (ST).

Composition	ST	Majority element		Minority element		Bond basins	
		Element	Charge	Element	Charge	No. × Charge	Shape
$F\bar{4}3m$							
$Li_{64.3}In_{26.5}Ag_{9.2}$	I	Li	+0.8 to +0.9	In/Ag	−1.6 to −0.8	None	
$Zn_{78-81}Pd_{14-16}Al_{4-8}$	I	Zn	+0.0 to +0.2	Pd	−1.2 to −0.6	None	
				Al	+1.2 to +1.3		
$Li_{81.0}M_{19.0}$	I	Li	∼ +0.8	M	−3.7 to −3.1	4× (−0.3 to −0.1)	Triangular
				(M = Pb, Sn, Ge)			
$Zn_{77-83}Pt_{17-23}$	I	Zn	+0.1 to +0.4	Pt	−1.1 to −0.9	None	
$Cu_{76-80}Sn_{23-24}$	I	Cu	−0.1 to −0.0	Sn	+0.2 to +0.3	None	
$Zn_{89-92}Ir_{8-11}$	I/II	Zn	−0.1 to +0.4	Ir	∼ −1.2	None	
$Na_{86.3}Tl_{13.7}$	II	Na	+0.0 to +0.6	Tl	−2.8 to −2.4	None	
$Sc_{86.3}Os_{13.7}$	II	Sc	−0.4 to +1.1	Os	−3.5 to −3.4	41× (−0.4 to −0.3)	Bilateral
$Mg_{85-88}TM_{12-15}$	II	Mg	−0.8 to +1.4	TM	−6.8 to −4.6	6× (−1.3 to −0.4)	p/h
				(TM = Ru, Rh, Ir, Pd)			
$Zn_{95.3}Mo_{4.7}$	II	Zn	−0.2 to +0.8	Mo	−0.2 to +0.1	None	
$Al_{65.3}Cu_{18.1}Cr_{16.6}$	II	Al	+0.3 to +0.7	Cr/Cu	−2.3 to −0.6	None	
$Zn_{78-87}TM_{13-22}$	II	Zn	−0.1 to +0.2	TM	−0.4 to −0.1	None	
				(TM = Fe, Ni)			
$In_{54.5}Pd_{29.3}Ce_{16.3}$	II′	In	−0.3 to +0.2	Pd	−1.0 to −0.8	None	
				Ce	+1.3 to +1.4		
$Zn_{67.5}Ce_{16.7}Mg_{15.8}$	II′	Zn	−0.8 to −0.2	Ce/Mg	+1.1 to 1.4	None	
$Mg_{83.6}Gd_{16.4}$	III	Mg	−0.5 to +0.4	Gd	+0.3 to +0.6	17× (−0.5 to −0.2)	Bilateral
$Cd_{80.4}Sm_{19.6}$	III	Cd	−0.5 to −0.1	Sm	+1.2 to +1.3	None	
$Al_{63.6}Ta_{36.4}$	III	Al	−0.1 to +0.4	Ta	−0.6 to +0.3	15× (−0.2)	Bilateral
$Mg_{82.4}Y_{9.0}Ce_{8.6}$	III	Mg	−0.6 to +0.6	Y	∼ +0.9	31× (−0.8 to −0.1)	Diverse
				Ce	+0.2 to +0.4		
$Na_{49.2}Ba_{28.8}Li_{22.0}$	III′	Na	−0.4 to +0.1	Ba	−0.1 to +0.3	65× (−4.0 to −0.0)	Diverse
				Li	∼ +0.8		
$Na_{49.1}Sn_{26.3}In_{24.6}$	IV	Na	+0.7 to +0.8	In	−0.6 to −0.4	None	
				Sn	−1.1 to −0.9		
$Fd\bar{3}m$							
$In_{70.7}K_{29.3}$		In	−0.3 to −0.0	K	∼ +0.7	None	
$Ga_{47-54}M_{29-32}TM_{6}$ to 22		Ga	−0.6 to −0.0	M	+0.7 to +1.5	None	
				(M = Na, Li, Mg)			
				TM	−0.6 to −0.1		
				(TM = In, Cd, Ag, Cu)			
$Zn_{61.0}Ca_{35.6}Ni_{3.4}$		Zn	−1.0 to −0.5	Ca	∼ +1.2	None	
				Ni	∼ −0.4		

quasicrystals with different constituents and different atomic concentrations, because they are electron compounds with similar electron-per-atom ratios. The pseudogap formation in the density of states across the Fermi level E_F can be explained in two possible ways; one is by the interaction between the quasi-Brillouin zone (q-BZ) boundary and the Fermi sphere (FS), *i.e.* the Hume–Rothery mechanism (HRM), and the other is by *sp-d* hybridization (Fujiwara & Yokokawa, 1991; Mizutani, 2011; Friedel, 1988; de Laissardière *et al.*, 1995). A pseudogap near the Fermi energy reduces the total band energy. Due to the almost spherical symmetry of the q-BZs the HRM works most effectively in icosahedral quasicrystals. In aluminium transition-metal quasicrystals, the *d* states of a transition metal element are strongly hybridized with the *s* and *p* states of Al. This *sp–d* hybridization further enhances the pseudogap formed by the q-BZ-FS interaction. The deep pseudogap in the vicinity of E_F is a contribution to the stabilization of icosahedral quasicrystals.

The electronic density of states (*DOS*) as well as its projection onto the orbitals of the atoms were calculated as implemented in the *VASP* package. The projection scheme is not perfect; the sum over all projections does not add up to the total of the *DOS*. This is due to the fact that *VASP* does not use localized orbital basis sets but plane waves as the basis for the electron density. Hence the projected *DOS* is calculated by weighting the *DOS* with the projected integrated partial charges, integrated over the volumes of the 'atomic spheres'. As space cannot be filled by spheres completely, there will always be some discrepancy and the projected *DOS* just gives a qualitative picture.

The *DOS* was calculated for a group of representative structures of the $cF(464 - x)$ class. The *DOS* graphs are shown in Fig. 19 in the relevant range around the Fermi level. All structures show a clear metallic behavior, *i.e.* with significant electron density at the Fermi level. The plots are obviously very diverse on first glance. On closer inspection, most calculated *DOS* have a pseudogap in the proximity of the Fermi level E_F.

The *DOS* of all calculated structures shows a strong tendency to form dense spiky peaks. Theoretical (Fujiwara *et*
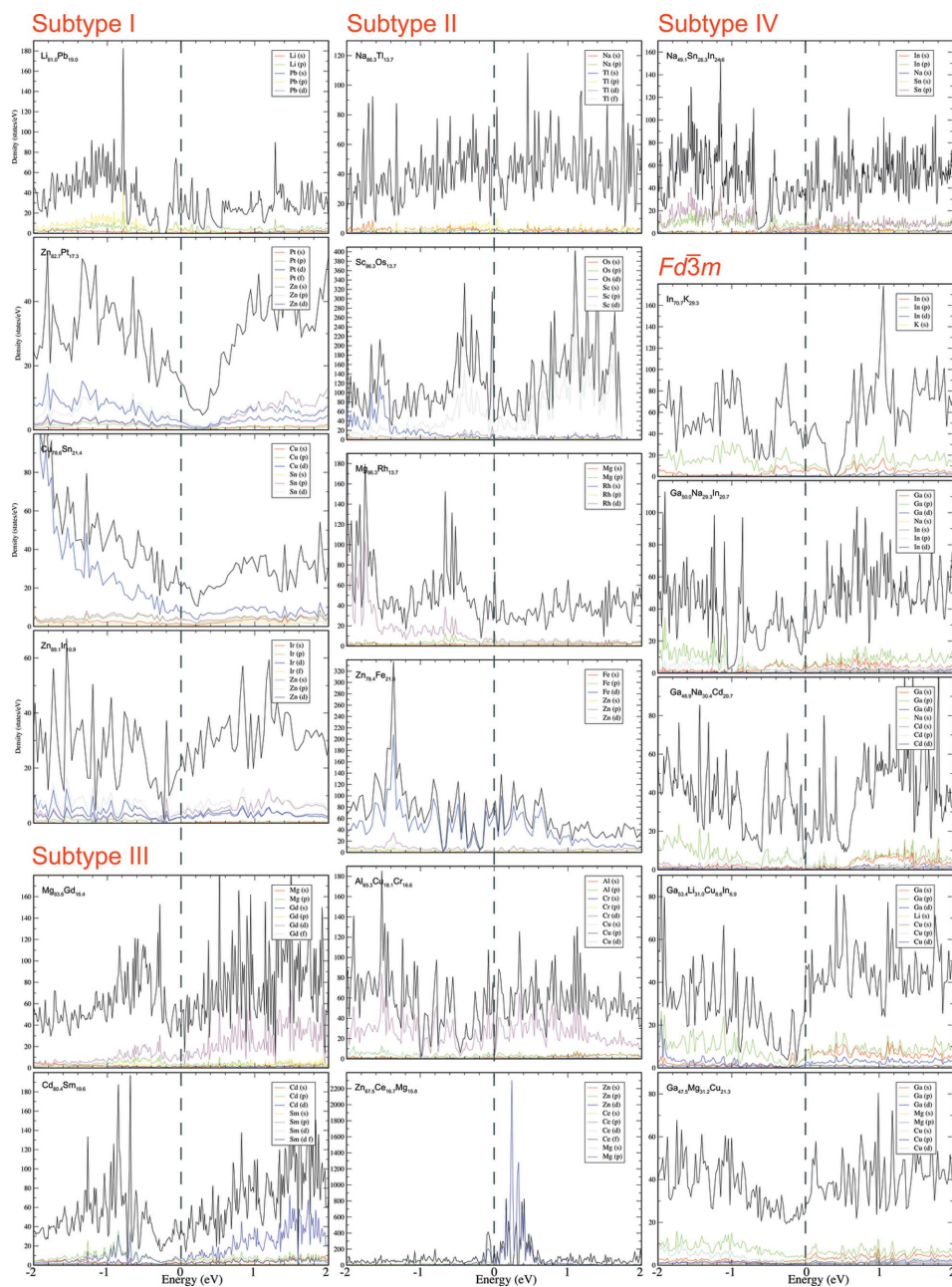
Figure 19
Density of states graphs for representatives of the investigated structures [$cF(464 - x)$]. Shown is the area between -2 and 2 eV; the Fermi level is denoted as a dashed line. The density axes are scaled differently, which is legitimate due to the difference in number of electrons in the various systems.

Finally, a word of caution has to be issued when addressing the *DOS* calculations and their interpretation with respect to all compounds. Due to the inherent periodicity and absoluteness of the atoms in the density-functional theory calculations used here, it is very hard to calculate structures with mixed-atom positions. On the other hand, if the mixed occupancy is ordered and can be described in a superstructure it can be calculated, but of course with a largely increased amount of computing time due the non-linear scaling of density functional theory calculations. Hence all structures with disorder or mixed occupancies on certain positions have been idealized, *i.e.* the occupancies have been rounded to zero or to one. For structures in real space this may have minuscule differences, but it can influence the *DOS* at specific points. Especially when dealing with transition metal compounds, the addition or subtraction of certain atoms and their respective electrons in the *d* orbitals changes the *DOS* near the Fermi surface and can move the position of the pseudogap along the *DOS*.

As already mentioned, the *DOS* at the Fermi surface and the pseudogap may vary from the real measured structures; this is mostly a result of the varying occupancy of the *d* states of the transition metals. The overall features of the *DOS* will however remain unchanged, as can be seen for instance when comparing $Ga_{53.4}Li_{31.0}Cu_{8.6}In_{6.9}$ and $Ga_{47.5}Mg_{31.2}Cu_{21.3}$ in Fig. 6 of the supplementary material, which differ in their composition only through the exchange of Mg with Li.

In the following we discuss the *DOS* of the structures according to their subtypes in the idealization, as listed in Tables 27 and 28 of the supplementary material. An interesting point here is that in general, the *DOS* of the structures are very diverse. This is astonishing as the principle building scheme of the structures is the same. Only when comparing structures which are in the same subtype and have a similar

al., 1994; Hippert *et al.*, 1999) and experimental (Escudero *et al.*, 1999) studies on quasicrystals and their structure approximants have observed a similar spikiness in their *DOS*. These spiky features could be associated with the confinement of electrons in clusters (de Laissardière & Mayou, 1997), and lead to a spiky *DOS* with the involvement of many clusters. An assembly of the complete *DOS* plots is shown in Fig. 6 of the supplementary material.

composition (at least when considering the number of electrons involved in bondings), like $Zn_{82.7}Pt_{17.3}$ and $Zn_{89.1}Ir_{10.9}$ in subtype I, are the overall characteristics of the *DOS* the same, but one can clearly see the effect of the different number of electrons in the *d* states, leading to a different *DOS* at the Fermi energy and shifting the pseudogap above the Fermi energy for $Zn_{82.7}Pt_{17.3}$.

6.3.1. Subtype I. In the *DOS* of $cF420$-$Li_{81.0}Pb_{19.0}$, the pseudogap at approximately -0.2 eV from E_F is very pronounced, while just above it an energetically unfavorable maximum arises at the Fermi level. Taking a partial occupancy of the Pb sites into account (Goward *et al.*, 2001), the Fermi level could be lowered into this pseudogap. Thus, *via* vacancies and disordered sites, the structure may tune the *DOS* to the most favorable configuration. The *DOS* of two more representatives of subtype I, $cF(416 - 16)$-$Zn_{82.7}Pt_{17.3}$ and $cF(416 - 4)$-$Cu_{78.6}Sn_{21.4}$, exhibit clear pseudogaps at approximately $+0.2$ eV. The heavily disordered compound $cF(452 - 36)$-$Zn_{89.1}Ir_{10.9}$ again features a very narrow but deep pseudogap at *ca* -0.2 eV.

6.3.2. Subtype II. The two isostructural subtype II compounds $cF408$-$Na_{86.3}Tl_{13.7}$ and $cF408$-$Sc_{86.3}Os_{13.7}$ exhibit very spiky *DOS* with a couple of minima which could be interpreted as pseudogaps. $cF408$-$Mg_{86.3}Rh_{13.7}$ and $cF408$-$Zn_{78.4}Fe_{21.6}$ show distinct pseudogaps at around -0.2 eV. The *DOS* of $cF(412 - 28)$-$Al_{65.3}Cu_{18.1}Cr_{16.6}$ has a very narrow and deep gap located directly at the Fermi level. In the *DOS* of $cF480$-$Zn_{67.5}Ce_{16.7}Mg_{15.8}$ the significant contribution of the Ce-*f*-states has its onset at around -0.2 eV. A broad and low minimum can be observed approximately at the Fermi level,

6.3.3. Subtypes III and IV. The *DOS* of $cF444$-$Al_{63.6}Ta_{36.4}$ has already been shown by Conrad *et al.* (2009) and another representative of subtype III, $cF(448 - 4)$-$Mg_{83.6}Gd_{16.4}$, also does not exhibit any clear features around E_F. In the very spiky *DOS* of $cF448$-$Cd_{80.4}Sm_{19.6}$, a broad pseudogap can be found at around -0.3 eV and a rather narrow one at approximately $+0.1$ eV. The only structure belonging to subtype IV, $cF456$-$Na_{49.1}Sn_{26.3}In_{24.6}$, is again quite spiky and has a very narrow pseudogap at E_F; the broad minimum at -0.6 eV could be interpreted to be a pseudogap as well.

6.3.4. $Fd\bar{3}m$. $cF464$-$In_{70.7}K_{29.3}$, the only binary compound in the group of $cF464$ structures crystallizing in space group $Fd\bar{3}m$, exhibits an actual gap in the *DOS* at $+0.4$ eV. The *DOS* of $cF444$-$Ga_{50.0}Na_{29.3}In_{20.7}$ exhibits a striking pseudogap at -1.0 eV, while two less deep ones are found at -0.6 and -0.1 eV. The *DOS* of $cF(464 - 4)$-$Ga_{48.9}Na_{30.4}Cd_{20.7}$ shows a pseudogap directly at E_F. The *DOS* of $cF464$-$Ga_{53.4}Li_{31.0}Cu_{8.6}In_{6.9}$ shows a significant rise of the overall level at the Fermi level; just below, at -0.1 eV, a pseudogap can be found. No hint towards any pseudogaps, however, can be found in the *DOS* plot of $cF(464 - 13)$-$Ga_{47.5}Mg_{31.2}Cu_{21.3}$.

7. Conclusions

The most striking result of our analysis of f.c.c. complex intermetallics with giant unit cells is that all of them follow the same building principles regardless of significant differences in chemical composition and bonding. The structures discussed here are mainly binary (29) and ternary (26), with one quaternary compound also included. The unit-cell dimensions seem to be determined by the type of layer structure under the constraint of cluster formation, as well as the size of the fundamental clusters and their packing principle.

The packing appears to be stabilized by an energetically favorable stoichiometry, which is specific for a certain system; many of the binary compounds, for example, have compositions of around $A_{85}B_{15}$. The respective composition then makes the formation of a simpler structure in the phase diagram impossible, but instead allows for a simple packing of bigger structural units – the clusters – which are more flexible with regard to composition.

Another interesting result is that all these structures can be seen as p^3-fold superstructures with $p = 3, 4, 7$ or 11 depending on their lattice parameters. The underlying basic structure of the $cF16$-NaTl-type is indicated by the set of most intense Bragg peaks in their diffraction patterns. This means that the slightly puckered atomic layers of the average structure are not only strongly scattering X-rays but also electrons, which can lead to pseudogaps in the *DOS*. Indeed, almost all structures in all subtypes display pseudogaps in the vicinity of the Fermi energy and a very spiky *DOS*.

It is also remarkable that the structures can also be interpreted as topological layer structures. The number of one flat and $p - 1$ puckered (110) layers per period equals p, the period in the superstructure description. The three-dimensional framework of interpenetrating layer stackings along all six symmetrically equivalent [110]-directions determines the kind of clusters and their packing that is compatible with it. The cluster structure found builds by decoration and puckering of the layers, whereas the cluster centers again mostly arrange on atomic positions corresponding to a $cF16$-NaTl-unit cell.

To summarize, intermetallic compounds are prone to form giant unit cells if their odd stoichiometry favors the formation of clusters that pack in a way allowing the formation of a three-dimensional framework of atomic layers. The existence of an underlying basic structure is a consequence of these structural building principles.

References

Alvarez, S. (2005). *Dalton Trans.* **13**, 2209–2233.
Alvarez, S. (2006). *Dalton Trans.* **17**, 2045–2051.
Andersson, S. (1980). *Acta Cryst.* B**36**, 2513–2516.
Arnberg, L., Jonsson, A. & Westman, S. (1976). *Acta Chem. Scand. A*, **30**, 187–192.
Bader, R. F. W. (1990). *Atoms in Molecules – A Quantum Theory.* Oxford University Press.
Becke, A. D. & Edgecombe, K. E. (1990). *J. Chem. Phys.* **92**, 5397–5403.
Belsky, A., Hellenbrandt, M., Karen, V. L. & Luksch, P. (2002). *Acta Cryst.* B**58**, 364–369.

feature articles

Berger, R. F., Lee, S., Johnson, J., Nebgen, B., Sha, F. & Xu, J. (2008). *Chem. Eur. J.* **14**, 3908–3930.

Blase, W., Cordier, G. & Vogt, T. (1991). *Z. Anorg. Allg. Chem.* **606**, 79–90.

Blöchl, P. E. (1994). *Phys. Rev. B*, **50**, 17953–17979.

Bonhomme, F. & Yvon, K. (1995). *J. Alloys Compd.* **227**, L1–L3.

Booth, M. H., Brandon, J. K., Brizard, R. Y., Chieh, C. & Pearson, W. B. (1977). *Acta Cryst.* B**33**, 30–36.

Brunner, G. O. & Schwarzenbach, D. (1971). *Z. Kristallogr.* **133**, 127–133.

Chabot, B., Cenzual, K. & Parthé, E. (1980). *Acta Cryst.* B**36**, 2202–2205.

Chahine, A., Tillard-Charbonnel, M. & Belin, C. (1995). *Z. Kristallogr.* **210**, 80.

Conrad, M., Harbrecht, B., Weber, T., Jung, D. Y. & Steurer, W. (2009). *Acta Cryst.* B**65**, 318–325.

Cordier, G. & Müller, V. (1993a). *Z. Kristallogr.* **205**, 353–354.

Cordier, G. & Müller, V. (1993b). *Z. Kristallogr.* **205**, 133–134.

Cundy, H. M. & Rollett, A. P. (1961). *Mathematical Models.* Oxford University Press.

Escudero, R., Lasjaunias, J., Calvayrac, Y. & Boudard, M. (1999). *J. Phys. Condens. Matter*, **11**, 383–404.

Feuerbacher, M. *et al.* (2007). *Z. Kristallogr.* **222**, 259–288.

Fornasini, M. L., Chabot, B. & Parthé, E. (1978). *Acta Cryst.* B**34**, 2093–2099.

Fornasini, M. L., Manfrinetti, P. & Gschneidner, K. A. (1986). *Acta Cryst.* C**42**, 138–141.

Fredrickson, D. C., Lee, S. & Hoffmann, R. (2007). *Angew. Chem. Int. Ed.* **46**, 1958–1976.

Friedel, J. (1988). *Helv. Phys. Acta*, **61**, 538–556.

Fujiwara, T., de Laissardière, G. & Yamamoto, S. (1994). *Mater. Sci. Eng. A*, **179**, 118–121.

Fujiwara, T. & Yokokawa, T. (1991). *Phys. Rev. Lett.* **66**, 333–336.

Gómez, C. P. & Lidin, S. (2004). *Chem. Eur. J.* **10**, 3279–3285.

Goward, G. R., Taylor, N. J., Souza, D. C. S. & Nazar, L. F. (2001). *J. Alloys Compd.* **329**, 82–91.

Gribanov, A. V., Seropegin, Y. D., Bodak, O. I., Pavlyuk, V. V., Akselrud, L. G., Nikiforov, V. N. & Velikhovski, A. A. (1993). *J. Alloys Compd.* **202**, 133–136.

He, W., Zhang, J., Yan, J., Fu, Y. & Zeng, L. (2010). *J. Alloys Compd.* **491**, 49–52.

He, W., Zhang, J. & Zeng, L. (2007). *Powder Diffr.* **22**, 312–315.

Hellner, E. & Pearson, W. B. (1987). *Z. Kristallogr.* **179**, 175–186.

Henkelman, G., Arnaldsson, A. & Jónsson, H. (2006). *Comput. Mater. Sci.* **36**, 354–360.

Henley, C. F., de Boissieu, M. & Steurer, W. (2006). *Philos. Mag.* **86**, 1131–1151.

Hillebrecht, H., Kuntze, V. & Gebhardt, K. (1997). *Z. Kristallogr.* **212**, 840–847.

Hippert, F., Simonet, V., de Laissardière, G., Audier, M. & Calvayrac, Y. (1999). *J. Phys. Condens. Matter*, **11**, 10419–10450.

Hornfeck, W., Thimmaiah, S., Lee, S. & Harbrecht, B. (2004). *Chem. Eur. J.* **10**, 4616–4626.

Johansson, A. & Westman, S. (1970). *Acta Chem. Scand.* **24**, 3471–3479.

Koster, A. S. & Schoone, J. C. (1981). *Acta Cryst.* B**37**, 1905–1907.

Kreiner, G. & Schäpers, M. (1997). *J. Alloys Compd.* **259**, 83–114.

Kresse, G. & Furthmüller, J. (1996a). *Comput. Mater. Sci.* **6**, 15–50.

Kresse, G. & Furthmüller, J. (1996b). *Phys. Rev. B*, **54**, 11169–11186.

Laissardière, G. de & Mayou, D. (1997). *Phys. Rev. B*, **55**, 2890–2893.

Laissardière, G. T. de, Manh, D. N., Maagaud, L., Julien, J. P., Cyrot-Lackmann, F. & Mayou, D. (1995). *Phys. Rev. B*, **52**, 7920–7933.

Lee, S., Hoffmann, R. & Fredrickson, D. C. (2007). *Angew. Chem.* **119**, 2004–2023.

Lidin, S., Jacob, M. & Larsson, A.-K. (1994). *Acta Cryst.* C**50**, 340–342.

Lin, Q. & Corbett, J. D. (2005). *Inorg. Chem.* **44**, 512–518.

Mahne, S. & Harbrecht, B. (1994). *J. Alloys Compd.* **203**, 271–279.

Mizutani, U. (2011). *Hume–Rothery Rules for Structurally Complex Alloy Phases.* Boca Raton: CRC Press.

Monkhorst, H. J. & Pack, J. D. (1976). *Phys. Rev. B*, **13**, 5188–5192.

Nasch, T. & Jeitschko, W. (1999). *J. Solid State Chem.* **143**, 95–103.

Pavlyuk, V., Solokha, P., Zelinska, O., Paul-Boncour, V. & Nowik-Zając, A. (2008). *Acta Cryst.* C**64**, i50–i52.

Pavlyuk, V. V., Dmytriv, G. S., Tarasiuk, I. I., Pauly, H. & Ehrenberg, H. (2007). *Intermetallics*, **15**, 1409–1415.

Pecharskii, V. K., Bodak, O. I., Bel'skii, V. K., Starodub, P. K., Mokra, I. R. & Gladyshevskii, E. I. (1987). *Sov. Phys. Crystallogr.* **32**, 194–196.

Perdew, J. P., Burke, K. & Ernzerhof, M. (1996). *Phys. Rev. Lett.* **77**, 3865–3868.

Salamakha, P., Sologub, O., Bocelli, G., Otani, S. & Takabatake, T. (2001). *J. Alloys Compd.* **314**, 177–180.

Samson, S. (1962). *Nature*, **195**, 259–262.

Samson, S. (1964). *Acta Cryst.* **17**, 491–495.

Samson, S. (1965). *Acta Cryst.* **19**, 401–413.

Samson, S. (1967). *Acta Cryst.* **23**, 586–600.

Samson, S. (1972). *Acta Cryst.* B**28**, 936–945.

Samson, S. & Hansen, D. A. (1972). *Acta Cryst.* B**28**, 930–935.

Sikora, W., Malinowski, J., Kuna, A. & Pytlik, L. (2008). *J. Phys. Condens. Matter*, **104**, 012023.

Silvi, B. & Savin, A. (1994). *Nature*, **371**, 683–686.

Smetana, V., Babizhetskyy, V., Vajenine, G. & Simon, A. (2006). *Z. Anorg. Allg. Chem.* p. 2115.

Smith, A. P. & Ashcroft, N. W. (1987). *Phys. Rev. Lett.* **59**, 1365–1368.

Steurer, W. (2006). *Philos. Mag.* **86**, 1105–1113.

Stojanovic, M. & Latturner, S. E. (2007). *J. Solid State Chem.* **180**, 907–914.

Sugiyama, K., Saito, H. & Hiraga, K. (2002). *J. Alloys Compd.* **342**, 148–152.

Thimmaiah, S. & Miller, G. J. (2010). *Chem. Eur. J.* **16**, 5461–5471.

Thimmaiah, S., Richter, K. W., Lee, S. & Harbrecht, B. (2003). *Solid State Sci.* **5**, 1309–1317.

Tillard-Charbonnel, M. & Belin, C. (1992). *Mater. Res. Bull.* **27**, 1277–1286.

Tillard-Charbonnel, M., Chahine, A. & Belin, C. (1993). *Z. Kristallogr.* **208**, 372–373.

Tursina, A. I., Nesterenko, S. N., Noël, H. & Seropegin, Y. D. (2005). *Acta Cryst.* E**61**, i99–i101.

Villars, P. & Cenzual, K. (2009/10). *Pearson's Crystal Data.* Ohio: ASM International.

Weber, T., Dshemuchadse, J., Kobas, M., Conrad, M., Harbrecht, B. & Steurer, W. (2009). *Acta Cryst.* B**65**, 308–317.

Westin, L. & Edshammar, L.-E. (1971). *Acta Chem. Scand.* **25**, 1480–1481.

Westin, L. & Edshammar, L.-E. (1972). *Acta Chem. Scand.* **26**, 3619–3626.

Westin, L. & Edshammar, L.-E. (1973). *Chem. Scr.* **3**, 15–22.

Wolny, J., Kozakowski, B., Duda, M. & Kusz, J. (2008). *Philos. Mag. Lett.* **88**, 501–507.

Xiong, D.-B., Zhao, Y., Schnelle, W., Okamoto, N. L. & Inui, H. (2010). *Inorg. Chem.*, **49**, 10788–10797.

Yang, Q.-B., Andersson, S. & Stenberg, L. (1987). *Acta Cryst.* B**43**, 14–16.